

Article

Tectono-Paleogeographic Impact on the Permian Depositional Environment and Provenance around the Chaiwopu Depression in the Southern Junggar Basin, NW China

Shasha Liu ^{1,2,3} , Eun Young Lee ^{3,4,*} , Jinliang Zhang ^{2,*}, Michael Wagreich ³ , Leqiang Zhao ⁵ and Hui Liu ⁵

¹ Laboratory of Ocean and Coast Geology, Third Institute of Oceanography, Ministry of Natural Resources, Xiamen 361005, China; liushasha@tio.org.cn

² School of Natural Resources, Faculty of Geographical Science, Beijing Normal University, Beijing 100875, China

³ Department of Geology, University of Vienna, 1090 Vienna, Austria; michael.wagreich@univie.ac.at

⁴ Faculty of Earth Systems and Environmental Sciences, Chonnam National University, Gwangju 61186, Korea

⁵ Institute of Exploration and Development, Shengli Oilfield, SINOPEC, Dongying 257000, China; zhaoleqiang196.slyt@sinopec.com (L.Z.); liuhui988.slyt@sinopec.com (H.L.)

* Correspondence: eun.lee@univie.ac.at or eun.y.lee@chonnam.ac.kr (E.Y.L.); jinliang@bnu.edu.cn (J.Z.)

Abstract: The Chaiwopu Depression in the southern Junggar Basin is located between the West Bogda Mountains and the northeastern Tian Shan Mountains in northwest China. The intracontinental basin–mountain system was formed in the Central Asian Orogenic Belt during the Late Paleozoic. The Permian strata around the depression exhibits distinct variations, which provide significant information to understand its tectonic and depositional evolution. This study investigated six outcrop sites using lithological, sedimentological, and geochemical analyses. The representative lithology of the Lower Permian is submarine lava and pyroclastic flows on the northern margins and alluvial deposits near the southern margins. In the Middle Permian sequence, the extensive distribution of alternating shale and silt/sandstone with oil shale and carbonate indicates a lacustrine setting. The sediments are composed of felsic rock-forming minerals derived mainly from island arc settings. The source rock properties correspond to the Carboniferous volcanic terrain of northeastern Tian Shan. The Lower to Middle Permian source-to-sink system occurred in an incipient level of weathering and maturation, a simple recycling process, and arid to semi-arid climatic conditions. The characteristics and changes of the depositional environment and provenance can be understood in terms of implications of tectono-paleogeographic evolution associated with the West Bogda rifting and uplift.

Keywords: Chaiwopu Depression; West Bogda Mountains; southern Junggar Basin; northeastern Tian Shan; Central Asian Orogenic Belt; Permian; geochemical analysis; depositional environment; provenance; tectono-paleogeography



check for updates

Citation: Liu, S.; Lee, E.Y.; Zhang, J.; Wagreich, M.; Zhao, L.; Liu, H. Tectono-Paleogeographic Impact on the Permian Depositional Environment and Provenance around the Chaiwopu Depression in the Southern Junggar Basin, NW China. *Minerals* **2021**, *11*, 1237. <https://doi.org/10.3390/min11111237>

Academic Editors: David Gómez-Gras and Marta Roigé

Received: 7 October 2021

Accepted: 5 November 2021

Published: 8 November 2021

Publisher's Note: MDPI stays neutral with regard to jurisdictional claims in published maps and institutional affiliations.



Copyright: © 2021 by the authors. Licensee MDPI, Basel, Switzerland. This article is an open access article distributed under the terms and conditions of the Creative Commons Attribution (CC BY) license (<https://creativecommons.org/licenses/by/4.0/>).

1. Introduction

The Chaiwopu Depression is a sub-basin on the southern margin of the Junggar Basin in northwest China, which is about 115 km long from east to west and 35 km wide from south to north (Figure 1). It lies between the West Bogda Mountains, the Erenhabirga Mountains (branches of the northeastern Tian Shan Range), and the Turpan-Hami (Tuha) Basin. The series of intracontinental basins and mountains was formed by the amalgamation of multiple micro-continents, island arcs, and accretionary wedges, as part of the Central Asia Orogenic Belt (CAOB) (Figure 1a)—the largest accretionary orogen on Earth. Its formation process was associated with the closure of the Paleo-Asian Ocean. The Late Paleozoic has been considered as a significant period in the evolution of the intracontinental basin–mountain system. Extensive studies have been conducted to understand the complex tectonic evolution of the CAOB [1–16]. Sedimentary basins in the southern

CAOB, such as the Junggar, Tuha, and Tarim (Figure 1b), have received considerable geological attentions in past several decades, because they are important structures of the Late Paleozoic orogeny and rich in mineral resources [17–22]. In particular, high petroleum potential has been determined, due to the extensive distribution of source rocks showing high organic content [23,24]. The Chaiwopu Depression is located between major tectonic units (Figure 1b). Its outcrops, exposing relatively continuous Late Paleozoic strata, have been reported to be an important record of complex tectonic evolution. However, there are limited studies focusing on the Chaiwopu Depression compared to adjacent areas, which might be due to the complicated basin history and lack of geoscientific data and petroleum extraction potential [25]. It has remained a comparatively poorly investigated basin. This gap limits our understanding of the relationship between tectonic processes, depositional environments, and provenance in Permian time. Thus, in this study, we investigated lithological, sedimentological, and geochemical data acquired from six outcrop sites (Figure 1c) to understand the Permian evolution of the Chaiwopu Depression. Our results build on recent studies that established the Permian basin–mountain system of the Bogda Mountains and adjacent sedimentary basins [26–36].

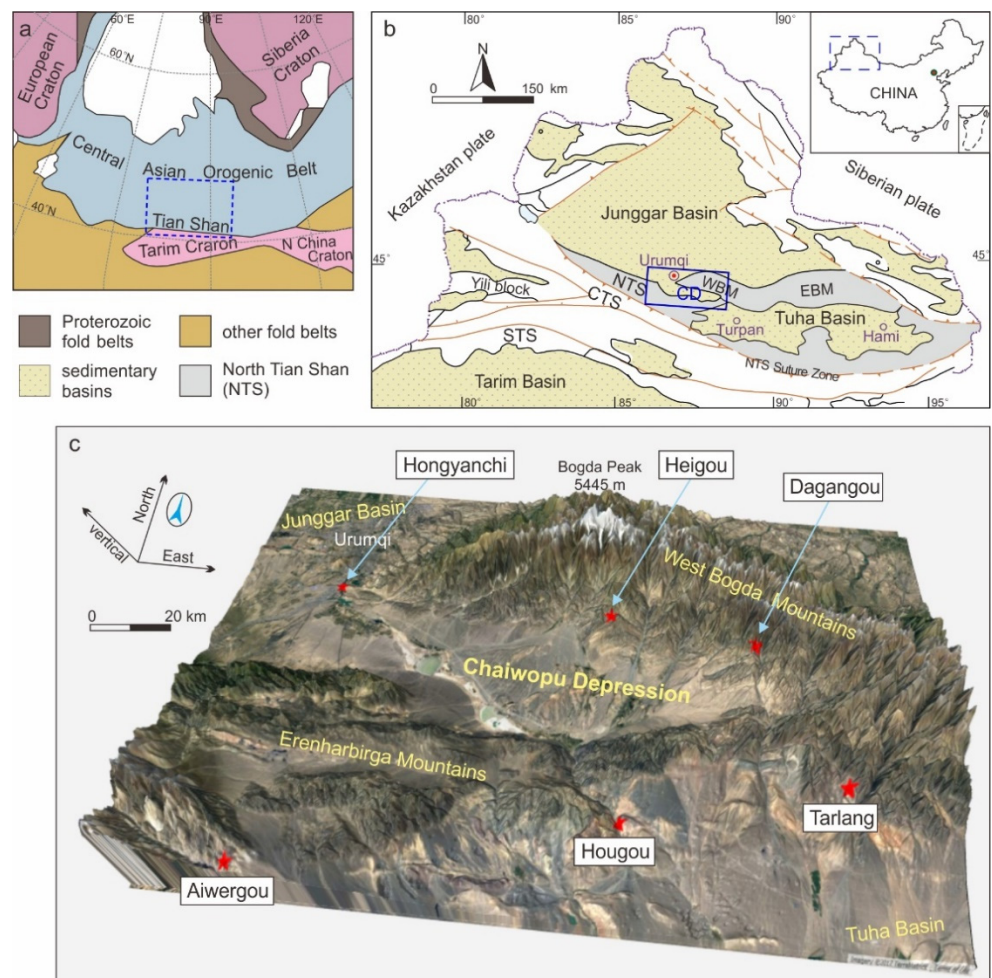


Figure 1. (a) Tectonic map of the Central Asian Orogenic Belt and adjacent tectonic units (after [2,5]). (b) Tectonic outline of northwest China (after [22]). The Chaiwopu Depression (CD) is located on the southern margin of the Junggar Basin. NTS—North Tian Shan (gray colored); CTS—Central Tian Shan; STS—South Tian Shan; WBM—West Bogda Mountains; EBM—East Bogda Mountains. (c) 3D visual map of the study area (blue square in (b)), using contemporary digital elevation model (DEM) data. Six outcrop sites (red stars) are shown.

The intracontinental basin–mountain series on the southern CAOB formed mainly during the Late Paleozoic as a derivation of the closure of the Junggar Ocean [4,16–18]. The formation of the Chaiwopu Depression is closely associated with the complex tectonic history of the southern Junggar Basin and West Bogda Mountains. During the Late Carboniferous to Early Permian, the Chaiwopu Depression was a part of the rifting West Bogda Trough. After the cessation of rifting at the end of the Early Permian, the area became a relatively stable tectonic setting with subsidence during the Middle Permian. The uplift of the West Bogda Mountains caused by strong intracontinental collision formed the basin geometry of the Chaiwopu Depression but restricted it from other major basins during the Late Permian [1,4,9,14–18,27,32,33,36]. The Permian successions around the Chaiwopu Depression provide a continuous and sensitive geological record reflecting the tectonic evolution and associated paleogeographic changes. In this study, we report on lithological, mineralogical, and sedimentary features of Permian sections at six outcrop sites, based on field observations, macroscopic and microscopic descriptions, and rock composition analyses using collected rocks samples. Geochemical analyses provide useful information to construct multiple discrimination diagrams. The relative ratios of major and trace element values were used to investigate various factors associated with lithology, tectonic setting, source rock properties, weathering degree, and climatic and environmental conditions [37–53]. This study aims to (1) identify the lithological, mineralogical, and sedimentary characteristics of the Permian strata; (2) interpret the depositional system, paleoenvironment, and provenance; and (3) reconstruct the Permian tectono-paleogeographic evolution of the Chaiwopu Depression.

2. Geologic Background

2.1. Tectonic Setting

The CAOB is surrounded by the European Craton to the west, the Siberian Craton to the northeast, the Tarim Craton to the south, and the North China Craton to the southeast (Figure 1a). It represents one of the most significant sites to understand Phanerozoic crustal growth on Earth and the closure of the Paleo-Asian Ocean [54–56]. It was shaped by the continuous amalgamation of micro-continental blocks, accretion wedges, volcanic arcs, seamounts, and oceanic plateaus in the Paleo-Asian Ocean from the Neoproterozoic to Late Paleozoic period. The Paleo-Asian Ocean included the Ob–Zaisan, Junggar–Balkhash, and Turkestan oceans from north to south [4,5,13,16–18]. In the Early Hercynian period (Devonian to early Carboniferous), the southern CAOB was folded by subduction, convergence, and collision of the NTS–Junggar–Turpan microplates. Sinistral strike–slip faults further deformed their structures. The Tian Shan mountain range is situated on the southern margin, located between the Junggar and Tarim Basins in present-day China (Figure 1b), extending more than 3000 km from northwestern China to Kazakhstan, Kyrgyzstan, and Tajikistan [5,10,12]. Based on the evidence of sutures in the field and geophysical data analyses, the Chinese Tian Shan evolved into three units: North Tian Shan (NTS), Central Tian Shan (CTS), and South Tian Shan (STS). The NTS, representing Late Paleozoic arc sequences, is distributed along the southern Junggar and Tuha Basins (Figure 1b).

From the middle Carboniferous to early Triassic, a complex interplate tectonic evolution formed the Junggar–Bogda–Tarim structures. The Bogda Mountains became an integral part of the northeastern Tian Shan orogenic belt, which separates the Junggar and Tuha Basins. The Late Paleozoic orogeny established a distinct geologic history in the West Bogda Trough to mountains and basin evolution [1,4,7–9,14,15,18,27,32,33,36], arranged as four major phases, as follows (Figure 2a): (1) During the middle Carboniferous to Early Permian, the extensional phase was initiated by mantle upwelling and regional crustal extension as a delamination effect of the post-orogenic collision period. This formed an intracontinental rifting system in the paleo Bogda area, which accompanied Early Permian bimodal volcanism and syn-tectonic plutonism. (2) At the end of the Early Permian, the rifting in the West Bogda Trough was closed as a result of the collision between the northern Junggar Block (Siberia Plate) and the southern Tarim Block. The West Bogda area shifted

to the intracontinental evolution stage, accompanying regional crust uplift and seawater regression. The orogeny created an embryo of the West Bogda Mountains. (3) During the Middle Permian, the area continued to subside, possibly due to the relaxation of compression and isostatic rebound of crustal deformation. It inherited the subsidence centers from the Early Permian. (4) At the end of the Middle Permian, strong intracontinental collision between the Junggar and Tarim Blocks caused the uplift of West Bogda Mountains. The paleostress changed from extensional to compressional kinematics. During the Late Permian, the N–S compressional stress facilitated the Bogda fold-and-thrust belt range in the eastern NTS. It formed an anticline structure bounded by thrust faults and local extrusion folds to the southernmost Junggar and Tuha Basins. It separated the Chaiwopu and Fukang Depressions. Differential uplifts over the area resulted in severe denudation of the Permian sediments.

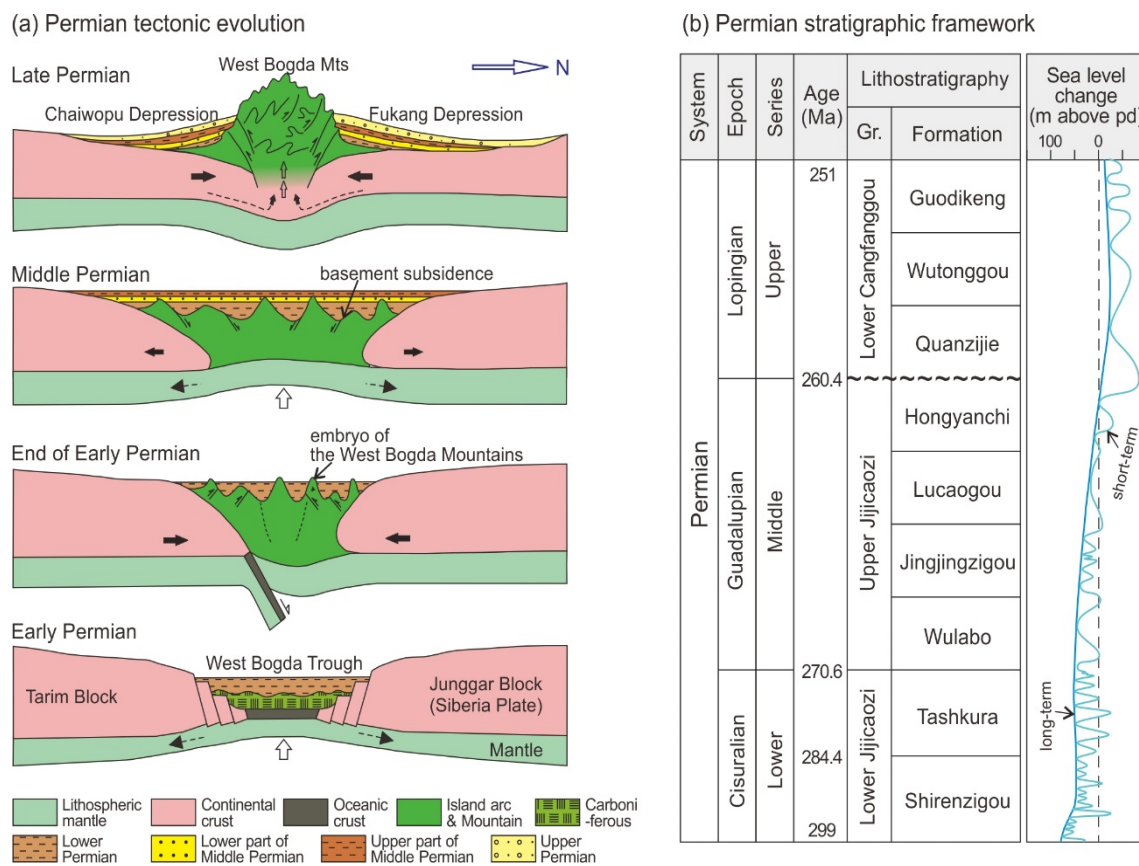


Figure 2. (a) Permian tectonic evolution model of the West Bogda Mountains (modified from [32]). (b) General Permian stratigraphic framework around the southern Junggar Basin and West Bogda Mountains [19,22,32,34,35]. Wavy line marks major unconformity. Sea level change curves in meters above the present-day (PD) shoreline are from [57].

2.2. General Stratigraphy of Permian Strata

Around the Chaiwopu Depression, the Carboniferous to Permian volcanic and sedimentary successions have been exposed (Figure 3). The Carboniferous sedimentary formations consist mainly of sandstone, mudstone, and limestone, deposited in marine environments [32,33]. The Permian strata are divided into lower, middle, and upper sequences. Each sequence contains several formations (Figure 2b), and those with different nomenclatures can be correlated over the southern Junggar Basin, Tuha Basin, and West Bogda Mountains. Here we summarize the general lithological and sedimentary characteristics of each formation, based on previous studies [18–26,28–35,58]. The Lower Permian volcano–sedimentary sequence (Lower Jijicaozhi Group, ca. 299–270.6 Ma) consists of the Shirenzigou and Tashkula Formations (Figure 2b), which formed during the Early

Permian extensional phase accompanied by growth faults and volcanic eruptions. The Shirengzigou Formation is composed mainly of shallow marine clastic and calcareous rocks. This sequence contains calcareous, lithic, and tuffaceous sandstone, siltstone, mudstone, conglomerates, and tuff layers. The Tashkura Formation is dominated by marine deposits. Alluvial conglomerates–sandstones and dolomite–limestone layers are present locally. The Lower Permian sequence is frequently intercalated or intruded by igneous rocks, including basaltic lava flows, tuff, volcanoclastics, pyroclastics, and dikes. The Middle Permian strata (Upper Jijicaozi Group, ca. 270.6–260.4 Ma) are divided into the Wulabo, Jingjingzigou, Lucaogou, and Hongyanchi Formations (Figure 2b). The Wulabo Formation is conformable to the underlying Tashkula Formation. It consists mainly of fine- to medium-grained feldspar sandstone and siltstone, interbedded by tuffaceous sandstone, tuff, shale, mudstone, and thin dolomite. The Jingjingzigou Formation is composed mainly of mudstone, siltstone, and sandstone successions, and occasionally contains volcanoclastic, tuffaceous, and calcareous layers. Cross, parallel, and wave ripple beddings and bioturbations are commonly described in the sandstone layers. The lower Middle Permian strata exhibit a transition from restricted marine to fluvial–lacustrine setting. The major lithology of the Lucaogou Formation is well-stratified shale, mudstone, and siltstone, occasionally with thin dolomite, limestone, and sandstone layers. Due to abundant organic-rich oil shale, it is well known as one of major source rocks in the Junggar Basin. The Hongyanchi Formation consists of shale and mudstone with thin siltstone, sandstone, limestone, marl, and oil shale layers. The upper Middle Permian strata have been interpreted as lake plain to deep lacustrine deposits. The Upper Permian strata (Lower Cangfanggou Group, ca. 260.4–251 Ma) are divided into the Quanzijie, Wutonggou, and Guodikeng Formations in the southern Junggar Basin (Figure 2b), which are incompletely preserved due to severe denudation. The Upper Permian rocks are unconformable to the underlying Middle Permian strata. The formations are composed mainly of conglomerate, pebbly sandstone, sandstone, siltstone, and mudstone, deposited in fluvial and shallow lacustrine settings.

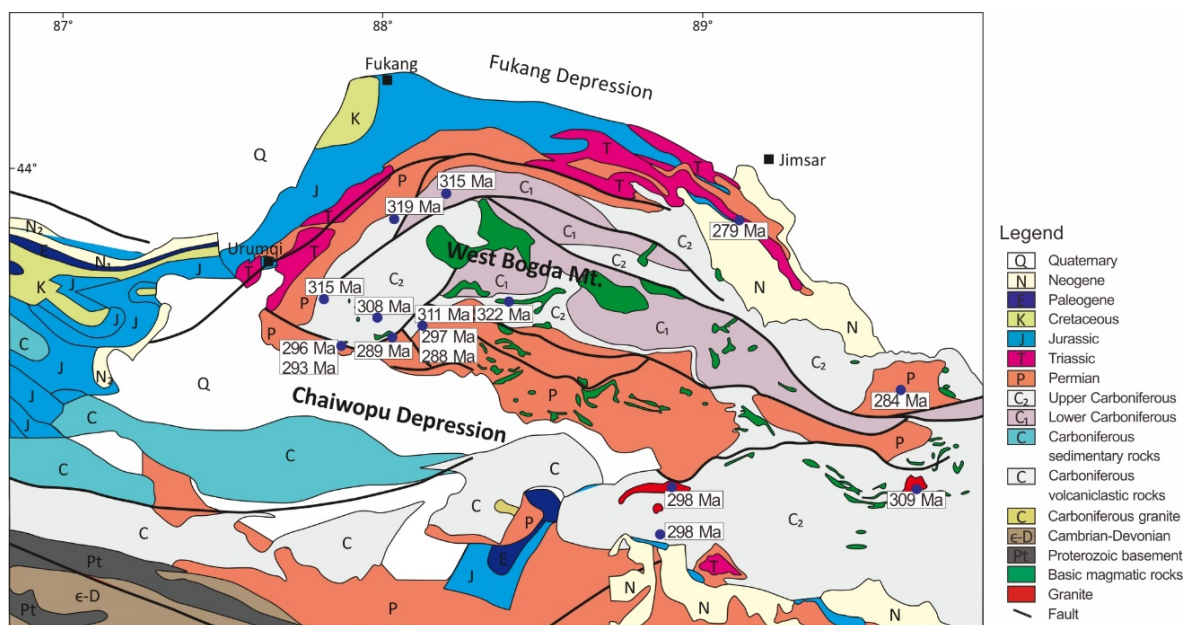


Figure 3. Geologic map of the Chaiwopu Depression, West Bogda Mountains, and adjacent areas (modified from [32]), showing the age data from [1,4,6,8,14].

3. Materials and Methods

3.1. Field Observation and Sampling

Field investigations were focused on 6 outcrop sites (Figure 1c). There are 3 sites located on the northern margin of the Chaiwopu Depression along the southern flank of the

West Bogda Mountains, as follows: Hongyanchi outcrop (HYC; 43°44'40" N, 87°38'18" E), Heigou outcrop (HEIG; 43°36'26" N, 88°23'25" E), and Dagangou outcrop (DGG; 43°32'48" N, 88°48'15" E), from west to east. The other 3 sites are in the Erenharbirga Mountains near the southern margin of the Chaiwopu Depression, as follows: Aiwegou outcrop (AWG; 43°00'52" N, 87°34'5" E), Hougou outcrop (HOUG; 43°11'16" N, 88°28'41" E), and Tarlang outcrop (TAR; 43°17'15" N, 89°2'47" E), from west to east. The structural and stratigraphic characteristics, including faults, unconformity, dikes, lithology, and thickness, were determined by field observations. Sedimentary structure, grain size, facies, and fossils were described based on field observations and sample analysis to interpret the depositional system and paleoenvironment. Samples were collected from rocks of representative and distinctive lithologies. Microscopic observations using the samples and thin-sections supplemented the sedimentary and mineralogical descriptions.

3.2. Analytical Methods

Lithological and mineralogical identifications of the rock samples were carried out at the Department of Geology, University of Vienna, Austria. The mineralogical features were examined by thin-section description and optical microscopy observation, combined with whole-rock X-ray diffraction (XRD) mineral identification. The XRD analysis was completed using a PANalytical PW 3040/60 X'Pert PRO X-ray diffractometer (CuK α radiation, 40 kV, 40 mA, step size 0.0167, 5 s per step).

A total of 22 samples were selected for bulk rock composition analysis (see Appendix Table A1 for sample information), including 12 samples from Lower Permian rocks and 10 samples from Middle Permian rocks. Major element data were obtained by X-ray fluorescence (XRF) spectrometry using fused glass disks, which were analyzed with a PANalytical AXIOS instrument at the Rock-Mineral Preparation and Analysis Lab, the Institute of Geology and Geophysics, Beijing, China. Loss on ignition (LOI) was measured as weight loss of the sample after 1 h of baking at a constant temperature of 1000 °C. USGS basalt and andesite standards (BCR-2, BHVO-1, and AGV-1) were used to indicate precision and accuracy better than 5% for major elements. Ferrous iron was determined according to titration methods [59]. Trace element data were detected by inductively coupled plasma atomic emission spectroscopy (ICP–AES). Rare earth elements (REE) were detected by inductively coupled plasma mass spectrometry (ICP–MS). These analyses were conducted at the testing center of Beijing Normal University, Beijing, China. For the examination, each 100 mg sample was soaked in a mixed solution of 10 mL HF, 10 mL HNO₃, and 2 mL HClO₄ in PTFE-lined, stainless-steel bombs at 200 °C for 48 h. The insoluble residues were dissolved at 130 °C by using 5 mL 30% (*v/v*) HNO₃ for 3 h and diluted to 25 mL. Standardized samples of GSS-1, GSS-2, GSD-7, and GSD-9, obtained from the Institute of Geology and Geophysics, Beijing, China, were used for calibration. The standard deviation for trace elements in the ICP–AES measurements was 0.002% and in ICP–MS was 0.0002%. The elemental composition data are provided as supplementary material in this study (Table S1).

We used the chemical index of alteration (CIA) to evaluate the chemical weathering degree. It is quantified as follows [46]:

$$\text{CIA} = \frac{\text{Al}_2\text{O}_3}{\text{Al}_2\text{O}_3 + \text{CaO}^* + \text{Na}_2\text{O} + \text{K}_2\text{O}} \times 100$$

where Al_2O_3 , CaO , Na_2O , and K_2O are molar values. The molar CaO is corrected to represent Ca silicate-bearing minerals only and excludes calcite, dolomite, and apatite (CaO^* ; [41]). The index of compositional variability (ICV) was used to evaluate the compositional and mineralogical maturity. It is defined as follows [39]:

$$\text{ICV} = \frac{\text{CaO} + \text{K}_2\text{O} + \text{Na}_2\text{O} + \text{Fe}_2\text{O}_3 + \text{MgO} + \text{TiO}_2 + \text{MnO}}{\text{Al}_2\text{O}_3}$$

where total iron is expressed as Fe_2O_3 and CaO involves all sources.

4. Lithological, Mineralogical, and Sedimentary Descriptions

At the six outcrop sites, Permian strata are apparently recognized between Carboniferous and Triassic rocks (Figure 4). The Upper Carboniferous rocks comprise volcano-sedimentary succession and rhyolite. Unconformity between the Upper Carboniferous and Lower Permian was observed at the HOUG outcrop (Figure 4e). Triassic rocks, consisting of conglomerate and sandstone, were observed at the TAR outcrop (Figure 4f).

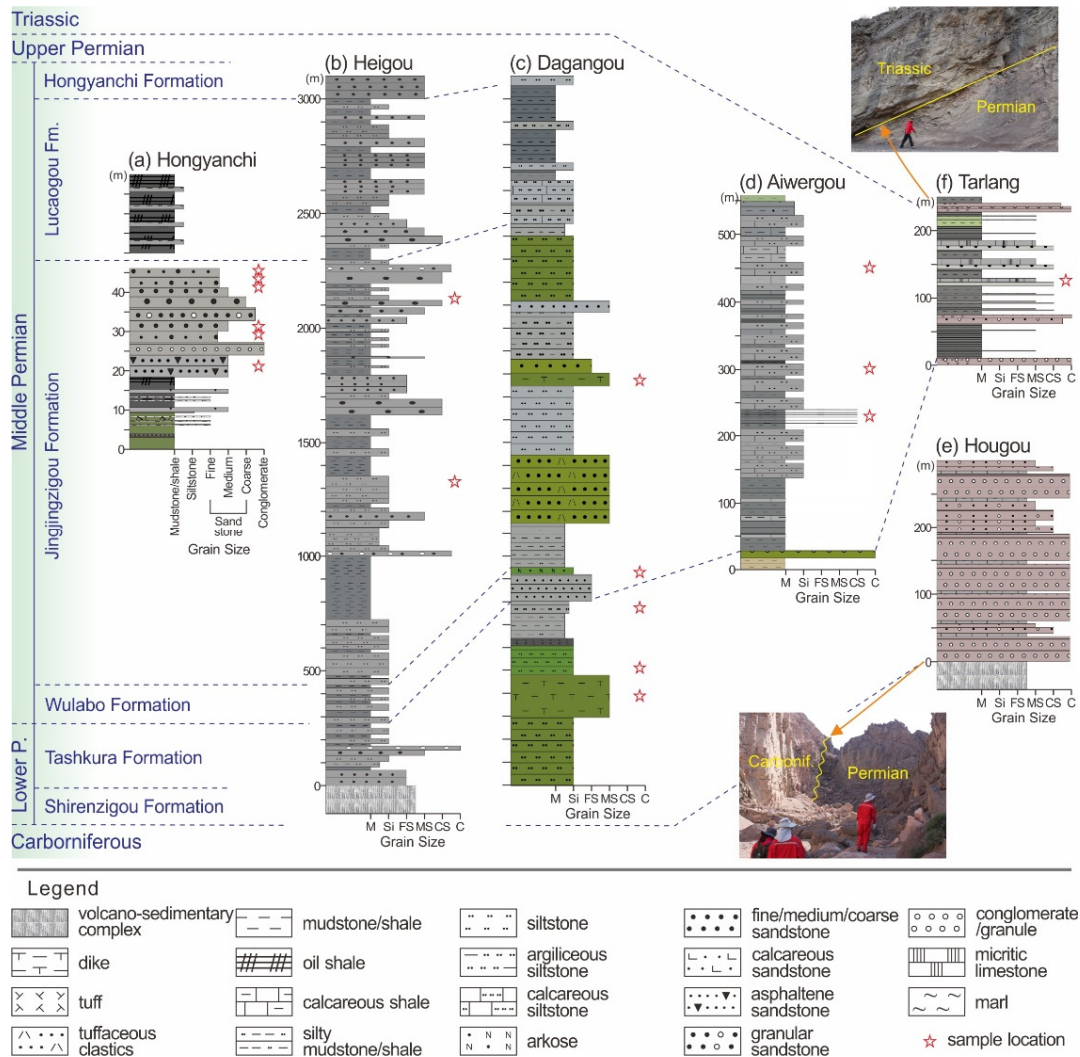


Figure 4. Stratigraphic correlation and representative lithofacies of six outcrop sections around the Chaiwopu Depression (See Figure 1c for outcrop locations). Colors in lithologic columns were selected to show rock colors as follows: light gray, gray, dark gray, blackish, greenish, and reddish or pinkish. Location of samples in Table A1 is shown (red stars). Sample locations from volcanic intrusions are not shown at the Hougou section. On the northern margin: (a) Hongyanchi section. Lithology between Jingjingzigou and Lucaogou Formations is uncertain due to poor exposure. (b) Heigou section and (c) Dagangou section. Boundary between Tashkura and Shirenzigou Formations is unclear. On the southern margin: (d) Aiwegou section. Formation boundaries of Middle to Upper Permian are not recognized. (e) Hougou section. Unconformity between Upper Carboniferous and Lower Permian is shown in field photograph. Boundary between Tashkura and Shirenzigou Formations is unclear. (f) Tarlang section. Formation boundaries of Middle to Upper Permian are not recognized. Contact with Triassic rocks is shown in field photograph.

4.1. Hongyanchi Outcrop

The HYG outcrop at the northwestern margin of the Chaiwopu Depression presents the Middle Permian Jingjingzigou and Lucaogou Formations (Figure 4a). The boundary

between these formations is uncertain due to poor exposure, but the formations show distinct lithological differences (Figures 4a and 5a).

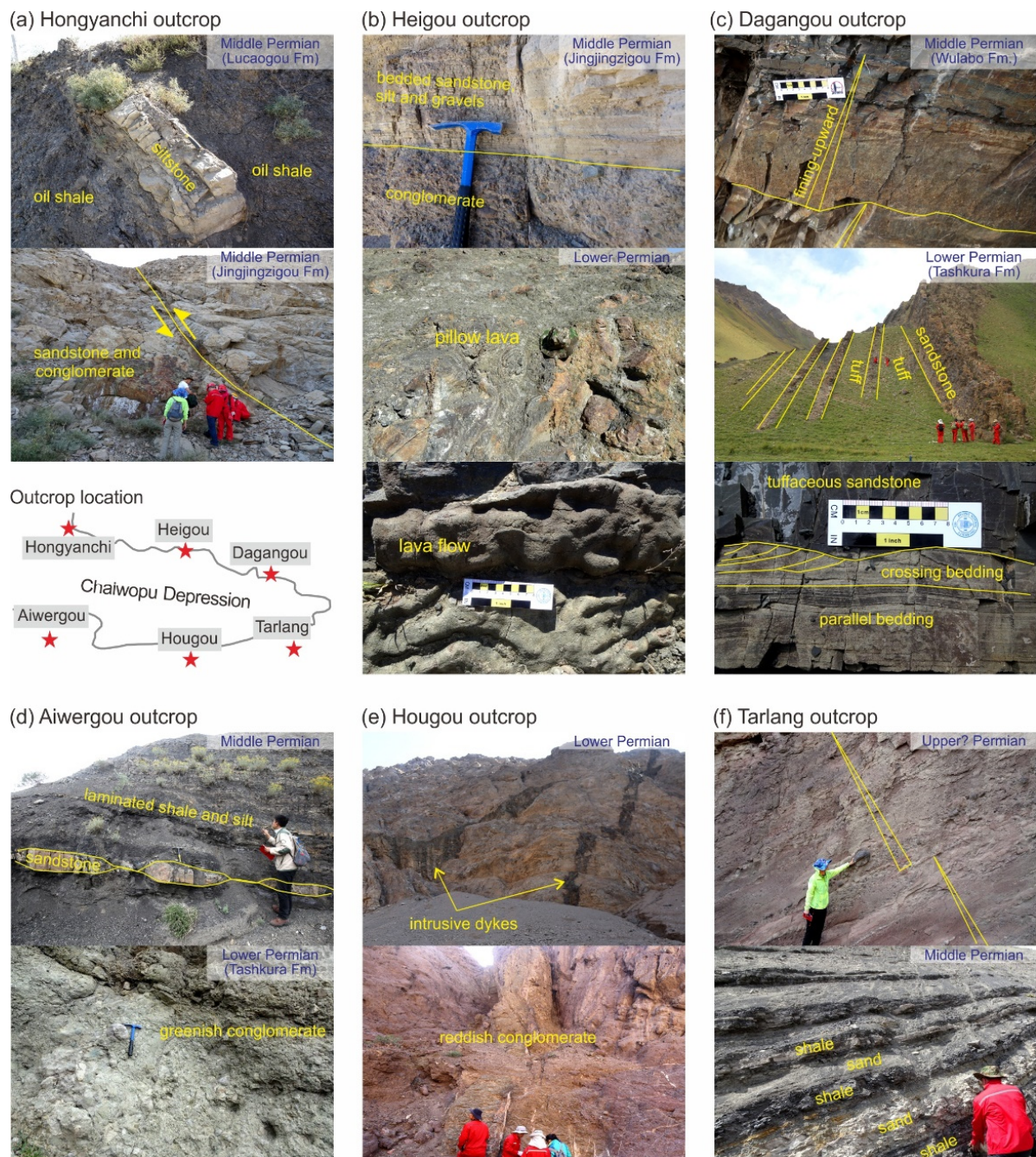


Figure 5. Representative field photographs. (a) Hongyanchi outcrop. Middle Permian with alternating oil shale and siltstone (Lucaogou Formation) and a sequence of sandstone–conglomerate with a fault (Jingjingzigou Formation). (b) Heigou outcrop. Middle Permian bedded sandstones with silt, gravel, and scouring surface of conglomerates (Jingjingzigou Formation). Lower Permian lava flows with pillow lava pile. (c) Dagangou outcrop. Middle Permian sandstone sequence with fining-upward cycles (Wulabo Formation). Lower Permian sequence of tuff and tuffaceous sandstone with beddings (Tashkura Formation). (d) Aiwegou outcrop. Middle Permian laminated shale and thin siltstone with interbedded lenticular sandstone. Lower Permian greenish conglomerates (Tashkura Formation). (e) Hougou outcrop. Lower Permian reddish conglomerates and intrusive dikes. (f) Tarlang outcrop. Upper? Permian pinkish fining-upward sandstone sequence with gravels. Middle Permian shale and sandstone sequence with thin gypsum and pyrite layers.

In the Jingjingzigou Formation, the lower section consists of greenish or dark gray mudstone and dark gray oil shale with thin calcareous or asphaltene sandstone layers. The major lithology of the upper section is grayish lithic medium- to coarse-grained sandstone, which contains granular, tuffaceous, and asphaltene sandstone and conglomerate layers (Figure 4a). Eight sandstone sets are described with faults (Figure 5a). The sandstone sequences, composed of abundant quartz and plagioclase (albite), show moderate to poor sorting, subangular grain shape, lithic/volcanic fragments, and some large, rounded quartz grains (Figure 6e). Siliceous and calcite cements are shown in cavities and pores. Brecciated and poorly sorted sandstone layers with angular volcanic clasts (0.5–1 mm) and lithic fragments (2–3 mm) are fractured, dissolved, and filled with siliceous, iron cements (Figure 6f). Some lithic sandstone layers contain grains floating in dissolved oil cavity with dry asphalt fluids, asphalt balls (1–2 cm), and oil patches, indicating residues of petroleum escape, which show poor sorting, angular to subangular grain shape, and lithic fragments including angular volcanic clasts (Figure 6g). Petrographic analysis of the sandstone samples shows ~45% lithic fragments and variable plagioclase and quartz contents (Figure 7a). Five samples are classified as arkose and one breccia sandstone as quartz arenite (Figure 7b). In the Jingjingzigou Formation, sedimentary structures in the sandstones are limited but suggest flow deposits, indicated by oriented grains, graded structure, and poor sorting with pebbles. Some interlayers show well-sorted and fining-upward sandstone and shales.

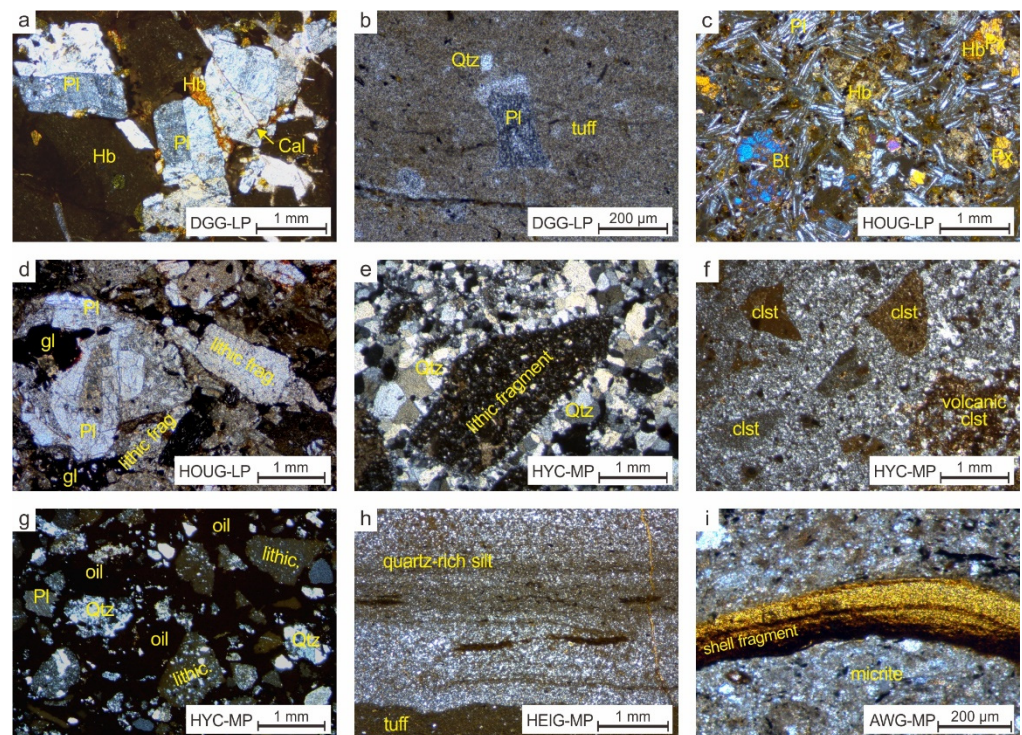


Figure 6. Thin-section images of Lower and Middle Permian samples. Lower Permian (LP): (a) coarse-grained diorite dike (sample DGG-10); (b) tuff with plagioclase and quartz fragments (sample DGG-03); (c) andesite dike (sample HOUG-04); (d) granular pyroclastics with plagioclase, lithic fragments, and glass (sample HOUG-05). Middle Permian (MP): (e) lithic sandstone (sample HYC-09); (f) breccia sandstone with volcanic clasts (sample HYC-10); (g) lithic sandstone with oil (sample HYC-05); (h) quartz-rich siltstone with tuff (sample HEIG-03); (i) detrital limestone with shell fragment and micrite (sample AWG-03). Pl—plagioclase; Qtz—quartz; Hb—hornblende; Cal—calcite; Bt—biotite; Px—pyroxene; gl—glass.

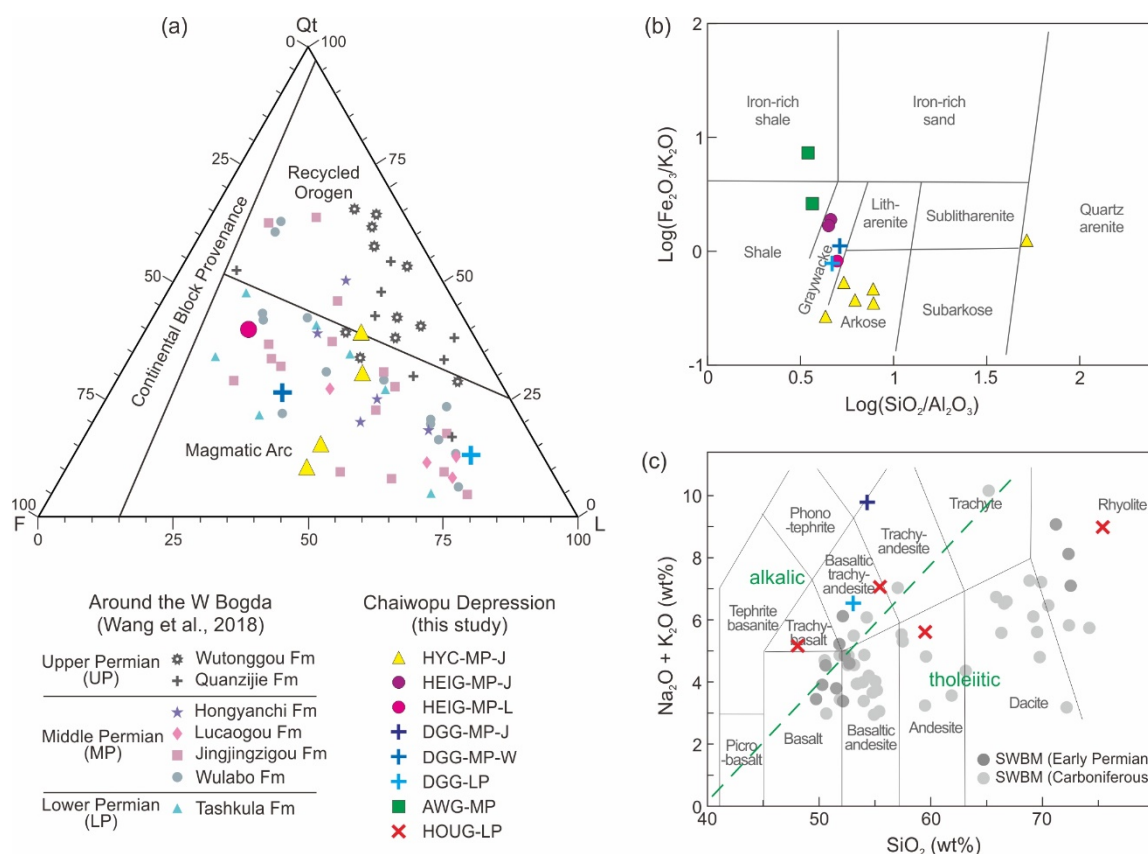


Figure 7. (a) Sandstone compositions in Dickinson ternary diagrams [40]. Samples from HYC, HEIG, and DGG outcrops are plotted. Data points for comparison are of Lower to Upper Permian samples from the West Bogda Mountains [32]. (b) Geochemical classification of sedimentary rock samples using $\log(\text{Fe}_2\text{O}_3/\text{K}_2\text{O})$ vs. $\log(\text{SiO}_2/\text{Al}_2\text{O}_3)$ diagram [43]. Data of sedimentary rock samples are plotted. (c) Total alkali ($\text{Na}_2\text{O} + \text{K}_2\text{O}$) vs. silica (SiO_2) diagram showing igneous rock classification [44]. Data of igneous rock samples collected from DGG and HOUG outcrops are plotted. Shown for comparison are data of Early Permian and Carboniferous igneous rock samples from the southwestern Bogda Mountains (SWBM) [4,6,14]. Sample information is provided as outcrop–age–formation. LP—Lower Permian; MP—Middle Permian; W—Wulabo Formation; J—Jingjingzigou Formation; L—Lucaogou Formation.

The Lucaogou Formation shows a rhythmic cycle of dark gray to black oil shale with thin laminae (0.5–1.5 m thick) and light yellowish-gray silt/sandstone (0.3–1 m thick) (Figures 4a and 5a). The oil shales contain organic-rich matter. The silt/sandstone shows muddy, fine, and uniform grain size with parallel, low-angle oblique, and cross beddings.

4.2. Heigou Outcrop

The HEIG outcrop in the north–central margin of the Chaiwopu Depression displays a complete section from the Lower to Middle Permian (Figure 4b). A large volume of basaltic–andesite lava flows represent the lower section of the Lower Permian, accompanied by pillow lava piles, pyroclastic flow and surge deposits, tuff, and tuffaceous clastics (Figure 5b). The Tashkura Formation consists of alternating gray mudstone, silty mudstone, and grayish siltstone. Grayish-yellow tuffaceous clastics and medium- to coarse-grained sandstone interbeds are extensively distributed. Mudstone layers (about 20–30 cm thick) are composed of quartz, plagioclase (albite), orthoclase, anorthite, and calcite. Occasionally, an E–W flow direction is indicated in sandstone layers with grain orientation and beddings. Mechanical deformation and weathering are observed.

The Wulabo Formation (~150 m thick) and the lowest section of the Jingjingzigou Formation are similar to the upper section of the Tashkura Formation (Figure 4b). The Jingjingzigou Formation (~1850 m thick) consists mainly of alternating stratified gray

shale and siltstone, which contains grayish fining-upward, fine- to coarse-grained or granular sandstone and occasional conglomerate interbeds (Figure 4b). The sandstone and siltstone interbeds, consisting mainly of quartz and plagioclase (albite), show weak parallel stratification, variable grain size, and cross, wavy cross, and trough beddings with ripples (Figure 5b). The quartz-rich siltstone shows an apparent boundary with tuff (Figure 6h). The lithological characteristics of the Lucaogou and Hongyanchi Formations are similar to those of the upper Jingjingzigou Formation but show decreased volcanic/lithic content. Samples collected from the Jingjingzigou and Lucaogou Formations are classified as graywacke (Figure 7b).

4.3. Dagangou Outcrop

The DGG outcrop displays Lower to Middle Permian strata on the northeastern margin of the Chaiwopu Depression (Figure 4c). In the Lower Permian section, a distinct difference from the HEIG outcrop is the absence of lava flows, but several intrusive dikes are present in the DGG. The dikes are continuous and extensive (about 0.5–1 m thick) and are classified as basaltic andesite (Figure 7c). They principally consist of plagioclase (70–80%), hornblende (5–10%), and pyroxene (mainly orthopyroxene), with minor alteration minerals such as albite, chlorite, calcite, and dolomite (Figure 6a). Plagioclase dissolution and fractures infilling calcite are observed. The boundary between the Tashkura and Shirenzigou Formations is unclear or not observed due to dikes. The Lower Permian sedimentary rocks are composed of siltstone, sandstone, tuff, and tuffaceous clastics with mudstone and conglomerate interbeds (Figure 4c). Volcanic glass, volcanic falling pieces, and lithic fragments are present. Relatively thick clastic beds are described as Bouma-like sequences, indicating turbidite deposition [60], which show a lateral but unstable continuity. In thinner beds, parallel and cross beddings with plant fragments are described (Figure 5c), implying a shallow marine environment. From bottom to top, the interbedded mudstone layers (0.2–2 m thick) become thinner and less frequent. Felsic tuff layers (0.3–0.5 m thick) are extensively distributed (Figure 5c) with mineral fragments of plagioclase (12–15%), quartz (10–15%), and minor alteration minerals such as calcite and hematite (Figure 6b; Table A1). Tuffaceous sandstone is classified as graywacke (Figure 7b).

The Middle Permian succession of the Wulabo and Jingjingzigou Formations consists mainly of siltstone and fine- to medium-grained sandstones. Quartz, plagioclase (albite), and minor calcite are predominant. In the Wulabo Formation, fining-upward sandstone sequences with volcanic clasts are observed (Figure 5c). Sandstones are composed of plagioclase (~40%), lithic fragments (30–35%), and quartz (25–30%) (Figure 7a), which are classified as graywacke (Figure 7b). Siltstone interbeds show ripples, beddings, and parallel laminae. In the Jingjingzigou Formation, siltstones show lamination, weak stratification, and tuffaceous sediments. Sandstone compositions are similar to those in the Wulabo Formation. Occasionally, argillaceous gravel lens and plant fragments are present. Cross, parallel, and convolute beddings with scouring are described. A few intrusive diorite dikes are continuously distributed (45–50 m thick), which are composed of coarse-grain plagioclase (35%), hornblende (35–40%), and pyroxene with plagioclase phenocryst (1–2 mm in size) and hornblende phenocryst (0.1–0.6 mm in size). The lower Lucaogou Formation consists of gray calcareous siltstone and shale. The upper section is predominantly dark gray shale with gray siltstone and sandstone interbeds (Figure 4c). Plane parallel, cross, and ripple beddings are occasionally shown with scoured contacts.

4.4. Aiwegou Outcrop

The AWG outcrop in the Erenharbirga Mountains (Figure 1c) shows the topmost Lower Permian to Middle Permian strata (Figure 4d). The presence of Upper Permian strata is unclear. The Tashkura Formation is composed of yellowish mudstone and greenish conglomerate. The massive conglomerates are poorly sorted, matrix- or grain-supported with sandstones (Figure 5d), and occasionally show fining- or coarsening-upward grade and cross bedding. The Middle Permian strata exhibit no distinct boundaries between

formations. Alternating gray to dark gray shale and gray siltstone deposits are extensively distributed with oil shale, calcareous or lithic siltstone (Figures 4d and 5d). The deposits are laminated or massive with a lack of sedimentary structures. Occasionally, thin marl, micritic or oolitic limestone, lenticular sandstone, conglomerate, and locally thin gypsum layers (1–2 cm) are interbedded. Two siltstone samples are classified as shale and iron-rich shale (Figure 7b). The calcareous clastics and detrital limestone layers are composed of calcite and quartz with abundant micrite grains and bioclasts derived from fish, bivalves, algae, and carbonized plant debris (Figure 6i).

4.5. Hougou Outcrop

The HOUG outcrop near the south-central margin of the Chaiwopu Depression exhibits Upper Carboniferous to Lower Permian strata with unconformity (Figure 4e). The Lower Permian volcano-sedimentary complex is mainly composed of basic and acidic igneous rock body (pinkish basalt–andesite and rhyolite; Figure 7c), intrusive grayish-green diorite dikes (each 1–3.5 m in width), massive reddish conglomerates, and sandstones (Figures 4e and 5e). Rhyolite shows a high quartz content with plagioclase (albite) and orthoclase. Andesite consists of plagioclase (~60%), hornblende (5–10%), and pyroxene (Figure 6c). Some plagioclase minerals show alteration states including kaolinitization. The hornblende minerals filling in between feldspar particles were partially altered into biotite minerals. Diorite porphyrite rocks of intrusive dikes (1–1.5 m in width) are broadly distributed in the region, and are composed of plagioclase feldspar (60%), hornblende (5–10%), pyroxene, and muscovite. The minerals show plagioclase phenocryst (0.5–3 mm), hornblende phenocryst (0.1–0.5 mm), and pyroxene crystal (0.3–0.8 mm), which are weakly altered and show calcite cements. The reddish conglomerates are massive, poorly sorted, and matrix-supported with volcanic clasts and fragments. Some intervals show imbrication, graded bedding, and sheet deposition. Large-scale reddish volcanoclastic rocks, including pyroclastic granules, present abundant quartz (0.5–2 mm in size), plagioclase (mainly albite), lithic fragments, and volcanic glass (Figure 6d). Subround to subangular gravels, pebbles, and lithics were mostly derived from igneous rock, tuff, and volcanic materials. Occasionally, thin mudstone, siltstone, gypsum, calcite interbeds, and sandstone lens are present, with parallel or cross bedding and fining-upward intervals.

4.6. Tarlang Outcrop

The TAR outcrop near the southeastern margin of the Chaiwopu Depression presents a sequence from Upper Carboniferous and Permian to Lower Triassic. The Upper Carboniferous to Lower Permian strata are similar to those in the HOUG outcrop (thus, their lithologic column is not shown in Figure 4f). The Middle–Upper Permian strata exhibit no distinct boundaries between formations. The Middle Permian succession consists of dark gray mudstone and shale laminae with interbeds of reddish or grayish conglomerate, sandstone, and gray limestone (Figures 4f and 5f). The deposits contain carbonate/dolomitic grains, lithics, pyrite, gypsum–marl, and organic matter. The uppermost Permian section, which might represent the Upper Permian strata, consists of reddish fining-upward sandstone sequences (Figure 5f). Each sequence exhibits an upward gradation from poorly sorted, matrix-supported pebbles and granules to well-sorted sandstones. The overlying Triassic succession consists of alternating conglomerate and sandstone with interbedded shale, limestone laminae, gypsum–marl, or dolomite.

5. Geochemical Characteristics

5.1. Tectonic Setting Analysis

We utilized a Zr/Y vs. Zr diagram to discriminate the magma source and tectonic setting of oceanic island arc, mid-ocean ridge, in the within-plate field [47]. Igneous rock samples from the DGG and HOUG were plotted, in which the samples present in or near the within-plate field can be seen (Figure 8). This is similar to the Carboniferous volcanic rocks in the Tian Shan [12]. For comparison, the data of igneous rock samples from the

southwestern Bogda Mountains [4,6,14] are plotted in the diagram. Early Permian samples are in or near the within-plate field, but Carboniferous samples show a spread from the island arc/mid-ocean ridge to within-plate fields (Figure 8).

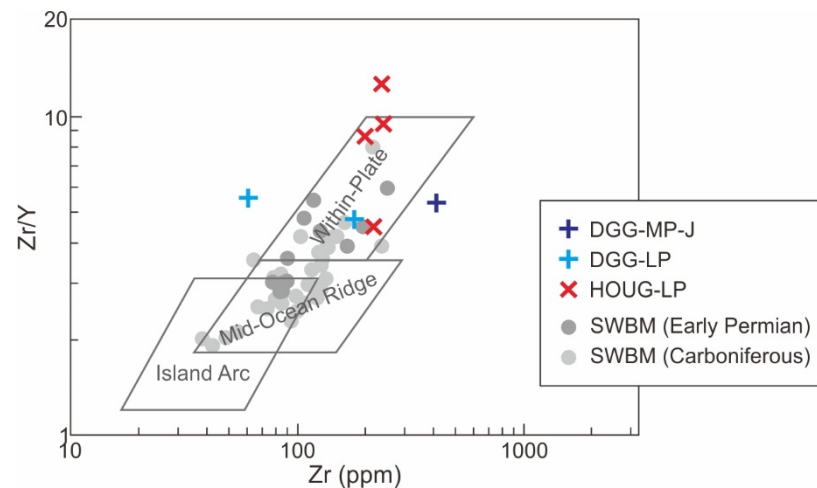


Figure 8. Zr/Y vs. Zr plot for different magma sources with distinct data fields for within-plate, mid-ocean ridge, and ocean island arc basalts [47]. Data of igneous rock samples collected from DGG and HOUG outcrops are plotted. Shown for comparison are data of Early Permian and Carboniferous igneous rock samples from the southwestern Bogda Mountains (SWBM) [4,6,14].

The geochemical diagrams, shown in Figure 9a–c, were utilized to discriminate the probable tectonic setting of the sediment source areas: oceanic island arc, continental island arc, active continental margin, and passive continental margin [37,38]. The plots provide information about the provenance, because the elements have weak activity and are difficult to dissolve in water. In a binary plot of Ti/Zr vs. La/Sc, the major paleo-tectonic setting is attributed to the discriminant zone of continental island arc (Figure 9a). One sample (HYC-10) lies in the oceanic island arc zone. On the other hand, in the La vs. Th diagram, all HYC samples are located in the oceanic island arc field (Figure 9b). Other samples are seen in or near the continental island arc and near the margin of active and passive continental fields. In the plot of the REE pattern normalized by post-Archean Australian shale (PAAS), the average pattern, evaluated using the samples in this study, is distributed near the continental and oceanic island arc patterns (Figure 9c). The discriminant function-based diagram proposed by [53] is used to identify the probable tectonic setting of the sediment source area (arc, rift, and collision). In both diagrams, for high-silica ((SiO₂)_{adj} = 63–95%) and low-silica ((SiO₂)_{adj} = 35–63%) samples, it can be seen that the data points are plotted in rift and arc fields (Figure 9d,e). Two HYC samples (HYC-11 and HYC-09) are near or at the border with the collision field.

5.2. Sediment Source Analysis

The discriminant function-based diagram in Figure 10a was used as a supplement to discriminate provenance types [50]. The Middle Permian samples of HYC and HEIG are seen in the felsic igneous and quartzose sedimentary provenance fields, while one DGG sample lies near the border between the felsic and intermediate igneous provenance fields. In the TiO₂ vs. Ni diagram [42], the plotting of data shows that the Permian rocks fall in the felsic source area (Figure 10b).

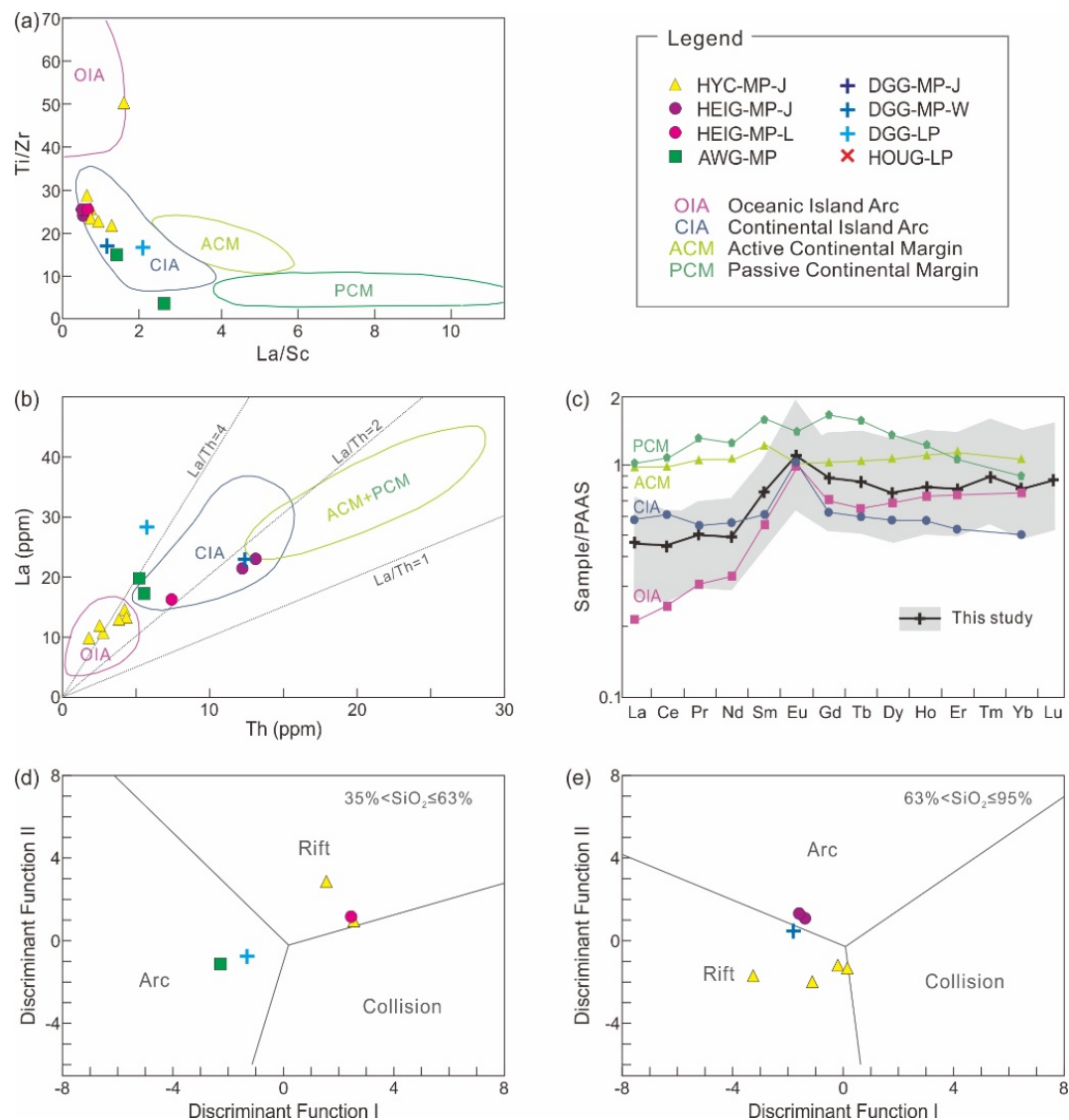


Figure 9. Binary plots to discriminate probable tectonic setting of sediment source area. **(a)** Ti/Zr vs. La/Sc and **(b)** La vs. Th for four distinct tectonic settings as follows: oceanic island arc (OIA), continental island arc (CIA), active continental margin (ACM), and passive continental margin (PCM) [38]. Data of sedimentary rock samples collected from study sites are plotted. **(c)** PAAS-normalized REE patterns for comparison with tectonic settings [37]. Patterns of sedimentary rock samples collected from study sites are shown in gray shade and their averaged pattern as a black crossed line. **(d,e)** show the discriminant function diagrams for high-silica ((SiO₂)_{adj} = 63–95%) and low-silica ((SiO₂)_{adj} = 35–63%) clastic sediments with rift, arc, and collision-related fields [53]. Sample information is provided as outcrop–age–formation. LP—Lower Permian; MP—Middle Permian; W—Wulabo Formation; J—Jingjingzigou Formation; L—Lucaogou Formation.

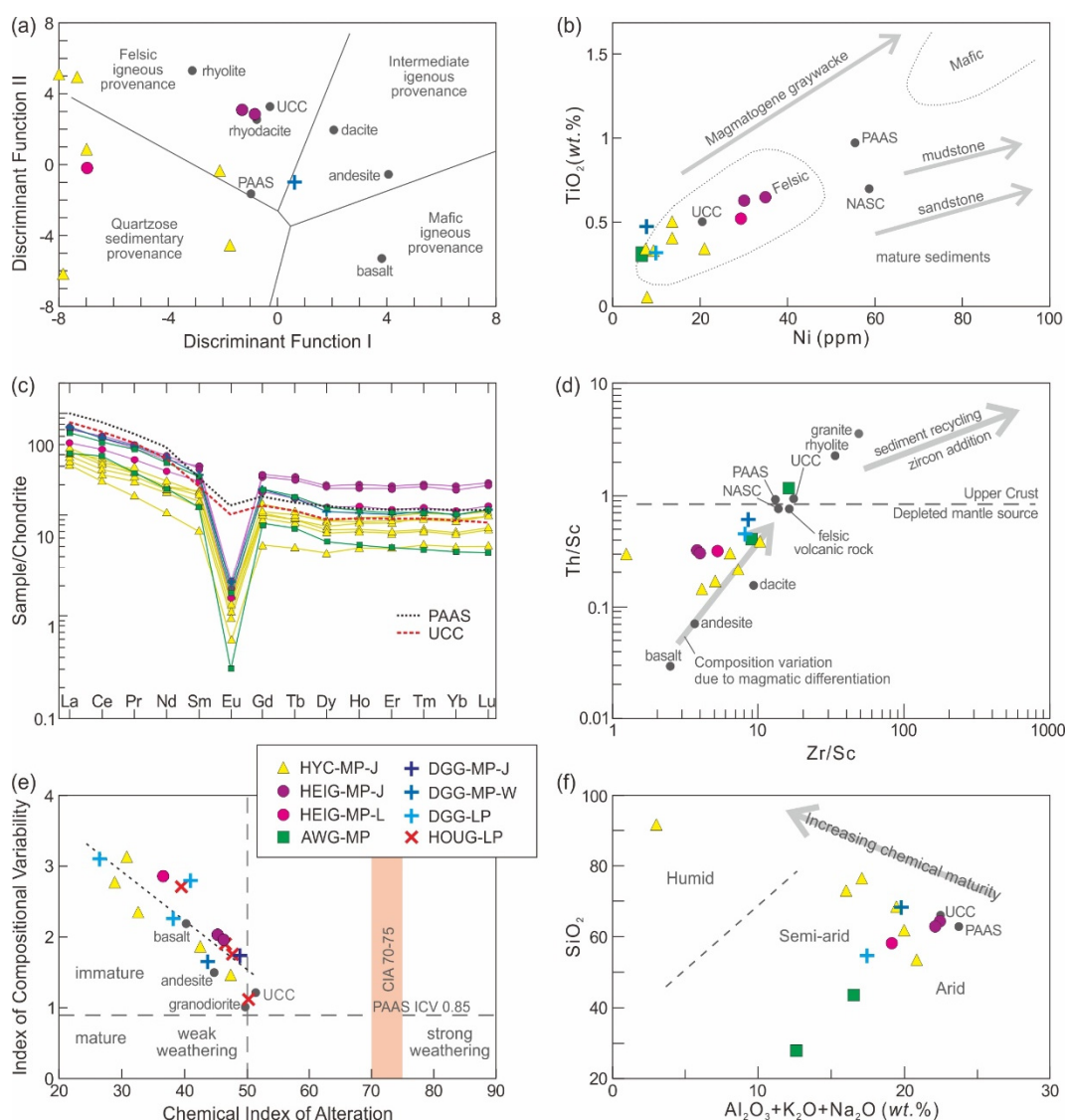


Figure 10. Binary plots to discriminate sediment source property, chemical weathering, and maturity. Data of rock samples collected from study sites are plotted. (a) Discriminant function diagram [50] and (b) TiO_2 vs. Ni plot for major source rock property and provenance [42]. (c) Chondrite-normalized REE element concentration patterns [37]. Patterns of PAAS and UCC are shown. (d) Th/Sc vs. Zr/Sc plot for discrimination of source rocks with directions of composition variation by magmatic differentiation and sediment recycling with zircon addition [45]. (e) Index of compositional variability (ICV) vs. chemical index of alteration (CIA) diagram for chemical weathering and maturity [3]. (f) SiO_2 vs. $\text{Al}_2\text{O}_3 + \text{K}_2\text{O} + \text{Na}_2\text{O}$ diagram for chemical maturity and paleoclimate [51]. UCC—average upper continental crust; PAAS—post-Archean Australian shale; NASC—North American shale composite [52]. Sample information is provided as outcrop–age–formation. LP—Lower Permian; MP—Middle Permian; W—Wulabo Formation; J—Jingjingzigu Formation; L—Lucaogou Formation.

The chondrite-normalized REE patterns for the Permian rocks are given in Figure 10c, together with those of PAAS and UCC (average upper continental crust) [52]. The incompatible REE elements are useful for discriminating source rock conditions due to their relatively low mobility during sedimentary processes and short residence time in marine environments. The Permian sedimentary samples show a consistent pattern, characterized by a slightly enriched light REE (LREE) and relatively flat heavy REE (HREE) profile with pronounced negative Eu anomalies (Figure 10c).

The Th/Sc vs. Zr/Sc diagram can be used to distinguish the contrasting effects between the source composition and sedimentary processes on the composition of sedimentary rocks [45]. Th to Sc ratio is very sensitive to compositional variations of the source

area, associated with igneous chemical differentiation processes. The Zr to Sc ratio reflects a trace of zircon enrichment in sediments, relative to Sc concentrated in mafic components. Zircon is a physically and chemically stable mineral, indicating the effect of sorting and recycling in sedimentary processes. In the case of Permian sedimentary rocks, it can be seen that the most samples follow a trend consistent with igneous differentiation (compositional variations) (Figure 10d), which reflects a close association with source rock properties and first-cycle deposition. Sample AWG-06 is present near the UCC. Sample HYC-10 is an outlier with regard to the magmatic differentiation trend.

5.3. Weathering and Maturity Analysis

The chemical index of alteration (CIA), used as a proxy to evaluate the degree of chemical weathering of sediments, reflects the weathering process of feldspar to aluminous clays [46]. The index is used to comprehend the weathering degree in the source region. The process is related to the paleoclimate, paleoweathering, and tectonism, which modify the chemical composition of rocks and sediments [41]. Generally, the CIA values of weakly weathered materials are below 50, which might reflect a cold and dry climate in the source terrain. Chemical weathering increases the value to 100, with clay formation, secondary mineralization, and textural changes. Strongly weathered source rocks and sediments are commonly related to hot and wet climatic conditions and hydrothermal activity [61,62]. The CIA values for the Permian igneous and sedimentary samples vary in a range from 26.4 to 50.1 (Figure 10e). These values suggest that the source terrains have been in a state of relatively fresh to weak weathering conditions. The geochemical composition of the sediments is potentially similar to that of the source materials.

The index of chemical variability (ICV; [39]), also shown in the diagram of Figure 10e, is employed to evaluate the compositional maturity of rocks and sediments. In general, ICV values >1 imply an immature source in the active tectonic setting, which contains rock-forming minerals such as pyroxene and feldspar, as well as first-cycle deposits of non-clay silicate minerals. Compositionally matured rocks or sediments with a high proportion of clay minerals, such as illite, muscovite, and kaolinite, show values <1 , which are attributed to recycled and chemically weathered sediments commonly in passive margin settings. The ICV values of the Permian samples are 1.1–3.1 (Figure 10e). This suggests that the rocks are compositionally immature and enriched in rock-forming minerals, indicating simply recycled sediments and weak weathering condition.

A binary plot of SiO_2 vs. $\text{Al}_2\text{O}_3 + \text{K}_2\text{O} + \text{Na}_2\text{O}$ by [51] was constructed to determine the chemical maturity and climatic conditions between humid and arid periods during the deposition of siliciclastic sediments. In this diagram (Figure 10f), data points of the Permian samples are plotted in the semi-arid and arid areas, except one sample (HYC-10) lies in the humid area. The Middle Permian HEIG samples are located near the UCC. This plot is further related to the SiO_2 to Al_2O_3 ratio, which is used as an indication of sediment maturity [48,49]. Higher values correspond to mature sediment, values <4 characterize immature sedimentation, values of 5–6 indicate progressive maturity, and values >7 mature sediment. $\text{SiO}_2/\text{Al}_2\text{O}_3$ values of the Lower to Middle Permian samples range from 3.2–7.9 (5.2 on average), indicating immature to submature conditions. A distinct outlier is the quartz arenite sample (HYC-10), with a value of 52.2 due to its high SiO_2 content (91.1%).

6. Discussion

Our results show the lithological, sedimentary, and geochemical characteristics of the Permian strata around the Chaiwopu Depression in the southern Junggar Basin. Their distinct variations correspond to paleogeographic configurations associated with the rifting and uplifting of the West Bogda area. We discuss our results to understand the transformation of the depositional environment and provenance conditions in response to tectono-paleogeographic evolution.

6.1. Depositional Environment

The Lower Permian strata on the northern margin area of the Chaiwopu Depression comprise volcano–sedimentary rock series (Figures 4b,c and 5b,c), corresponding to its location within the rifting West Bogda Trough during the Early Permian (Figure 11a) [32]. The rocks show a geochemical similarity to the Carboniferous to Early Permian volcanic rocks on the southwestern Bogda Mountains (Figures 7c and 8; [4,6,14]). At the HEIG outcrop, the presence of several basaltic–andesite lava flows and volcanoclastic deposits suggests multi-episode volcanic eruptions. Pillow lava piles and pyroclastic surge deposits indicate a subaqueous environment. Coarse clastic interbeds, showing flow direction and beddings, could have been deposited by slump on the volcano flanks (e.g., [63]). An overlying grayish succession of mudstone, siltstone, and fine-grained sandstone is reliably interpreted as deposition in a marine setting. At the DGG outcrop, extensive tuffs and tuffaceous clastic sequences with intrusive dikes are attributed to their farther distance from the volcanic sources. Varied sedimentary facies described in the sandstone sequences indicate dynamic morphological and bathymetric changes during the Early Permian. The Bouma-like and volcanic-rich sandstone sequences were likely deposited by turbidity currents at a relatively deep water depth, but thin sandstone layers with cross or parallel beddings imply shallow marine deposition. The Lower Permian volcanic rocks on the northern margin show textural deformation and secondary mineralization resulting from weathering and alteration, which are likely attributable to interactions between volcanic minerals and meteoric, seawater, and hydrothermal fluids (e.g., [62]). On the southern areas of the Chaiwopu Depression, sedimentary structures and facies provide limited information but suggest that massive conglomerates mixed with sandstones can be attributed to deposits in the alluvial fan system (e.g., [64]), which are commonly observed with the dynamic growth of normal fault zones in rift basins [65]. We infer that the southern areas were along the uplifted foothills and graben flanks in the extensional setting during the Early Permian (Figure 11a). The presence of graded sandstones with parallel, cross, or planar bedding suggests intervals of variable fluvial to shallow marine system. Occasional evaporite layers such as gypsum and calcite indicate a relation to the adjacent marine setting. The rapid variations in the depositional environment observed at both northern and southern areas demonstrate the active morphological controls by rifting and volcanic eruption (e.g., [64–66]) in addition to the eustatic sea-level change during the Early Permian (Figure 2b; [57]). The marine to fluvial depositional systems from north to south suggest that the West Bogda Trough was a relatively narrow deep-water basin with subaerially exposed rifted or tilted margins (Figure 11a).

At the end of the Early Permian, according to previous studies [6,13,17,32], the West Bogda Trough was closed and uplifted due to the collision of the Tarim and Junggar Blocks (Figure 11b). The kinematic change, with associated seawater withdrawal, induced an environmental change from a marine setting to a closed epicontinental offshore lacustrine [18,21,22]. It is verified that the shallow water sandstones of the Wulabo Formation directly overlie the deep-water mudstones of the Tashkula Formation in [32]; however, in our study, the lithology of the Wulabo Formation on the northern margin is fairly similar to the upper section of the Tashkura Formation (Figure 4b,c). This might reflect a progressive environmental transition in the trough during the latest Early Permian to earliest Middle Permian. In the southern areas, a sharp lithologic change from conglomerate to mudstone, shale between the Early and Middle Permian (Figure 4d,f) indicates increased water depth with an abrupt change in depositional setting.

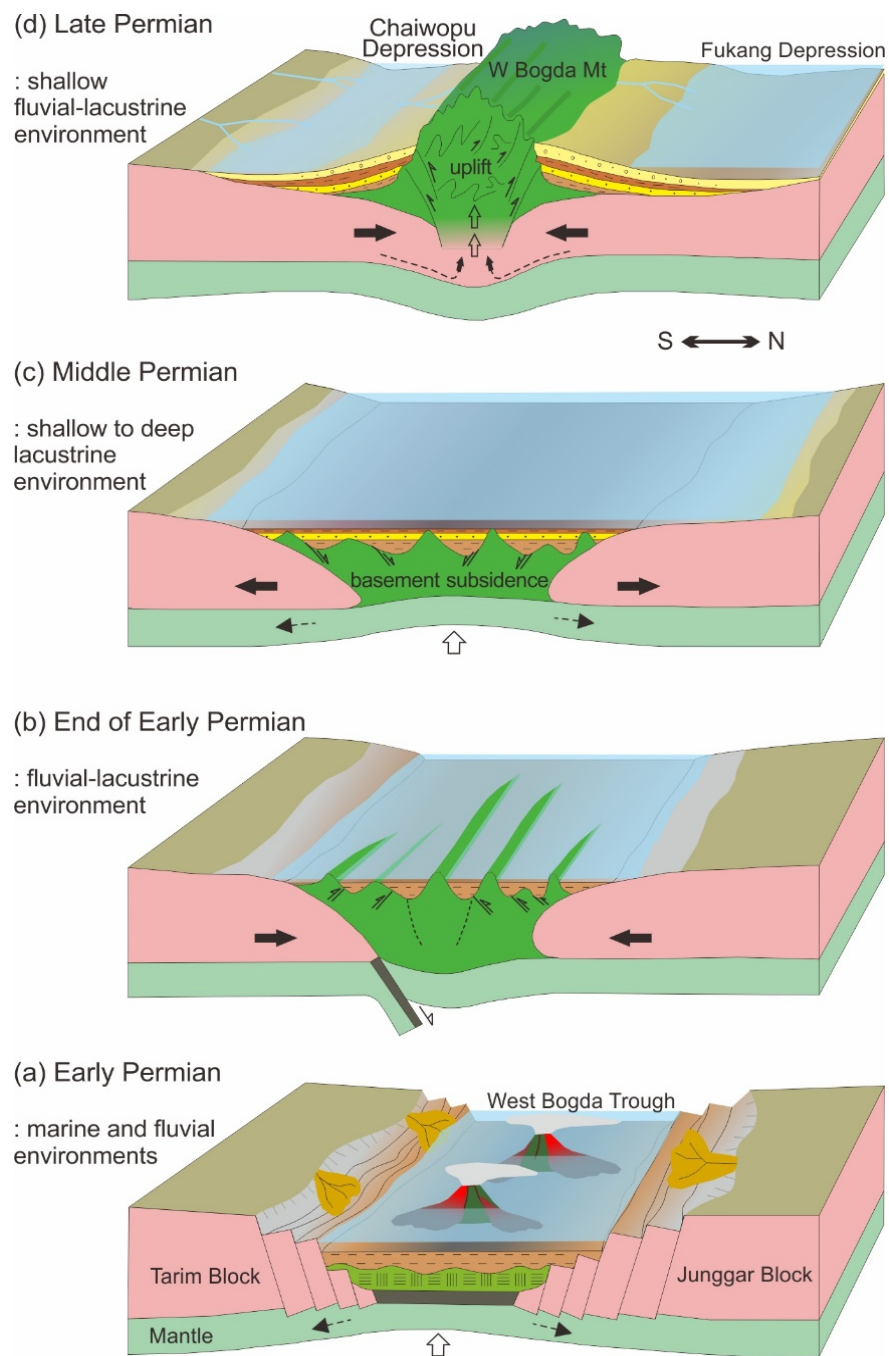


Figure 11. Tectono-paleogeographic evolution model with depositional environment settings around the Chaiwopu Depression and West Bogda: (a) Early Permian, (b) End of Early Permian, (c) Middle Permian, and (d) Late Permian. The tectonic evolution setting is based on [32] (see Figure 2a for legend). The depositional environment transitioned from marine and fluvial to closed epicontinental lacustrine at the end of the Early Permian. Extensive and shallow to deep lacustrine setting of the Middle Permian transitioned to shallow fluvial–lacustrine environment in the Late Permian.

In the Middle Permian, the predominant sedimentary facies of alternating mudstone–shale and silt–sandstone sequences correspond to the lacustrine depositional environment (Figure 11c). A widespread lacustrine setting has been described around the West Bogda Mountains and adjacent areas [19,21–26]. At the HEIG outcrop, the Middle Permian deposition is >2800 m thick with a >275 m/myr sedimentation rate. In particular, the Jingjingzigou Formation is extensively distributed and thick in the northern area. This

suggests that the lower Middle Permian sediments were deposited in a deepening basin with a large sediment supply. This corresponds to a subsidence inherited from the Early Permian [32], resulting from the relaxation of compression and isostatic rebound of crustal deformation, related to a high sedimentation rate (e.g., [67]). In this tectonic movement, distinct interbeds of the Jingjingzigou section, such as poorly sorted sandstone, conglomerate, or fining-upward sandstone layers, are likely derived from slump or flow deposition in a deep lacustrine transformation (e.g., [68]) or alluvial fan system on the paleo-Bogda Mountains [26,29].

The lower Middle Permian deposits can be interpreted as complex fluvial–lacustrine strata in a dynamic and partitioned basin [19,22,28,35]. The mixed deposits evolved upward into the fine-grained lacustrine facies of the upper Middle Permian, particularly the Lucaogou Formation. It shows a rhythmic cycling sequence of thin laminae and organic-rich shale with silt/sandstone. The alternation reflects changes between still–weak and weak–strong hydrodynamic settings. The shale characteristics indicate the static, deep, and anoxic to suboxic deep water lacustrine setting [23–25]. The silt/sandstone beds, showing muddy but uniform grain size with parallel, low-angle oblique, and cross beddings, could have been deposited at shallow lake margins during lake-level fall. This suggests that the upper Middle Permian lacustrine setting was relatively static but affected by lake-level fluctuations. This is also observed in the Middle Permian sections of the southern area. Lacustrine shale deposits with interbeds indicating fluvial influence or subaerial exposure reflect lake-level fluctuation in a shallow lacustrine and lake margin setting. At the TAR outcrop, the sedimentary characteristics of the upper sequences reflect a transition from a lacustrine to a fluvial-dominated environment during the late Middle Permian to Early Triassic. Similar changes have been reported in the southern Junggar and Turpan Basins [26]. According to [29], abrupt changes from the lacustrine–alluvial fan to the fan delta during the Middle to Late Permian are indicated around the West Bogda Mountains. These changes are attributed to a shallowing depositional environment with paleogeographic movements (Figure 11d), which could have been induced by the West Bogda uplift [29,32], a climatic disturbance [20,31], and/or an oversupply of clastic sediments relative to basin subsidence [22]. It might have been enhanced by the global sea-level fall in the Middle to Late Permian (Figure 2b; [57]).

6.2. Provenance

Petrographic analysis shows that the Lower to Middle Permian sandstone samples fall in the magmatic arc domain (Figure 7a; [29,32]). This corresponds to the mineral composition of our samples, which is genetically correlated with igneous rock components (Figure 6, Table A1). The volcanic fragments and tuffs are composed mainly of gravels, pebbles, and lithics in the Lower to lower Middle Permian sedimentary rocks. Their subangular shape and poor sorting suggest a relatively short distance of transportation from the source to the sink. In accordance with the comparison of geochemical compositions, the Permian sediments were controlled by a compositional variation of magmatic source rocks (Figure 10d). It is also believed that the sediments were predominantly derived from the adjacent felsic terrains (Figure 10a,b). The felsic-derived origin was likely inherited from the Carboniferous and Lower Permian igneous rocks of NTS and within the Bogda Trough [29,30,34,36]. The Late Carboniferous arc setting of NTS [4,8,11–15] corresponds to the major tectonic setting of sediment source areas in Figure 9a–c. This is supported by the presence of paleocurrents in the strata of the West Bogda [33], which are mainly north-directed, implying the provenance of sediments situated mainly to the south (Carboniferous volcanic-derived rocks) (Figure 3). Geochemical similarity to continental margin and rift settings (Figure 9c–e) is probably a result of the complex tectonic history and associated rock composition of the NTS, which might have derived from plate amalgamation, resident oceanic structure, volcanic eruptions, intrusive dikes, and regional extension [1,4,7–15].

After the cessation of rifting in the West Bogda Trough, materials related to proximal and synchronous magmatism, such as tuff and pyroclastics, decreased significantly in the

sediments. Since the volcanic clasts and lithics in the lower Middle Permian deposits were interpreted in terms of near-source sedimentation, the paleo-Bogda Mountains (Figure 11b) might have played a role as source rock until they were buried and/or denuded [26,30,34]. This corresponds to a decrease in volcanic materials upward in the Middle Permian sediments. However, despite the change and the variable paleogeographic configuration during the Lower to Middle Permian (Figure 11a–c), the chondrite-normalized REE patterns show little difference (Figure 10c). This demonstrates that the major provenance terrain, which is likely the NTS areas in the south of the Chaiwopu Depression, was subjected to a consistent source of a sink system with a simple recycling process. This is supported by the geochemical characteristics shown in Figure 10. According to previous studies [27,29,32], an abrupt change of provenance took place after the Middle Permian, which corresponds to re-sedimentation in the course of the uplift of the mountain range (e.g., [69]). The source rock properties of the Upper Permian are attributed to the recycled Middle Permian sediments from the West Bogda Mountains (Figures 7a and 11d; [29,32]).

The geochemical results in Figure 10, in addition to mineralogical characteristics, demonstrate that the Lower to Middle Permian source-to-sink system around the Chaiwopu Depression occurred in an incipient level of weathering, a simple recycling process, and arid to semi-arid climatic conditions. The low degree of weathering and maturation indicates relatively fresh source rock properties of proximal provenance in the NTS. On the chondrite-normalized REE plots, the Eu negative anomaly (Figure 9c) might imply significant chemical exchange during weathering and recycling. However, it could be derived from source rocks showing Eu negative anomalies related to plagioclase fractionation. The late Carboniferous to Early Permian rhyolites near the Chaiwopu Depression were reported to display similar patterns of chondrite-normalized REE with marked Eu negative anomalies in previous studies [1,6,8,15]. The rhyolite terrains are likely considered as the major provenance. Some Permian sediments on the northwestern Bogda Mountains show moderate weathering, submature conditions, and variable paleocurrents, which suggest different provenances [32,34,36]. This might explain the geochemical difference shown by sample HYC-10. The diverse weathering and maturation conditions around the West Bogda Mountains could have derived from a variety of source rock properties during dynamic tectono-paleogeographic movements.

7. Conclusions

This study reports the lithological, sedimentological, and geochemical characteristics of Permian igneous and sedimentary rocks around the Chaiwopu Depression in the southern Junggar Basin, northwest China. The findings were investigated to understand the depositional environment and provenance in response to Permian tectono-paleogeographic evolution. In the Early Permian, volcanic and sedimentary rocks in the northern area of the Chaiwopu Depression, which exhibit variations in the depositional system, were deposited in a marine setting. In the southern area, sedimentary rocks were deposited by alluvial fan and fluvial systems along the uplifted graben flanks. The characteristics of the Lower Permian rocks indicate active morphological and bathymetric changes in the rifting West Bogda Trough. At the end of the Early Permian, the marine setting turned to a fluvial–lacustrine environment by the uplift and cessation of rifting. The lower Middle Permian sediments were deposited at a high sedimentation rate in a subsiding basin. Extensive lacustrine deposition with lake-level fluctuations is significant in the upper Middle Permian. A bathymetric decrease in the Upper Permian and Early Triassic occurred mainly as a result of the West Bogda uplift, which changed the depositional environment to a shallow fluvial–lacustrine setting. The Lower to Middle Permian sediments show relatively uniform mineralogical and geochemical compositions. The felsic rocks of the NTS and within the West Bogda, likely rhyolites with a relatively short transportation distance, are suggested as the major provenance terrain. The low degree of weathering and maturity are associated with relatively fresh source rock properties, a simple recycling process, and arid to semi-arid climatic condition.

Supplementary Materials: The following are available online at <https://www.mdpi.com/article/10.3390/min11111237/s1>, Table S1: Elemental composition data of 22 samples listed in Table A1. Data were acquired by XRF, ICP-AES, and ICP-MS analyses. See Figure 4 for sample location.

Author Contributions: Conceptualization and methodology, S.L., E.Y.L., J.Z. and M.W.; validation, formal analysis, investigation, resources, data curation, S.L., E.Y.L., J.Z., M.W., L.Z. and H.L.; writing—original draft preparation, S.L., E.Y.L., J.Z., M.W., L.Z. and H.L.; writing—review and editing, S.L. and E.Y.L.; visualization, S.L. and E.Y.L.; supervision, J.Z. and M.W.; project administration, S.L., J.Z. and M.W.; funding acquisition, S.L., E.Y.L., J.Z. and M.W. All authors have read and agreed to the published version of the manuscript.

Funding: This research was funded by Hebei Provincial Funding Program for Returnees (No. C20190322) of China to S.L. and Brain Pool program through the NRF (2017H1D3A1A01054745) and Global R&D Activities through the WISSET by the Ministry of Science and ICT of Korea to E.Y.L.

Data Availability Statement: The data presented in this study are available in this article and supplementary material.

Acknowledgments: We acknowledge discussions with T. Choi and H. Lee on geochemical data interpretation. Special thanks go to colleagues of the Department of Geology, University of Vienna, for sample analyses, J. Wang for the figure file, and H. Jang for his artwork assistance.

Conflicts of Interest: The authors declare no conflict of interest. The funders had no role in the choice of research project; in the design of the study; in the collection, analyses, or interpretation of data; in the writing of the manuscript, or in the decision to publish the results.

Appendix A

Table A1. Twenty-two rock samples selected for bulk rock elemental composition analyses. Outcrop site, stratigraphy, formation, sample code, lithology, and major minerals are presented. Formations at the Aiwegou, Hougou, and Tarlang outcrops are unclear. MP—Middle Permian; LP—Lower Permian.

Outcrop	Strat.	Formation	Sample	Lithology	Major Minerals
Hong-yanchi	MP	Jingjingzigou	HYC-02	Lithic sandstone	quartz, plagioclase (albite)
			HYC-04	Lithic sandstone	
			HYC-05	Lithic sandstone with oil	
			HYC-09	Lithic sandstone	
			HYC-10	Breccia sandstone	
			HYC-11	Lithic sandstone	
Heigou	MP	Jingjingzigou	HEIG-03	Siltstone with tuff	quartz, plagioclase (albite), orthoclase
			HEIG-05	Lithic siltstone	
		Lucaogou	HEIG-07	Mudstone	quartz, plagioclase (albite, anorthite), orthoclase, calcite
Dagan-gou	LP	Tashkura	DGG-01	Altered diorite dike	plagioclase (albite), orthoclase, hornblende, pyroxene, chlorite, calcite, dolomite
			DGG-03	Tuff	
			DGG-06	Tuffaceous silt/sandstone	
	MP	Wulabo	DGG-07	Sandstone	quartz, plagioclase (albite), calcite
		Jingjingzigou	DGG-10	Coarse grained diorite	
Aiwer-gou	MP		AWG-03	Micritic limestone	calcite, quartz, plagioclase (albite), ankerite
			AWG-05	Lithic siltstone	
			AWG-06	Lithic siltstone	

Table A1. Cont.

Outcrop	Strat.	Formation	Sample	Lithology	Major Minerals
Hougou	LP		HOUG-02	Diorite porphyrite	plagioclase (albite, anorthite), hornblende, pyroxene
			HOUG-03	Rhyolite	
			HOUG-04	Andesite	plagioclase (albite, anorthite), hornblende, pyroxene, biotite
			HOUG-05	Granular pyroclastics	quartz, plagioclase (albite), hematite
Tarlang	MP		TAR-07	Detrital limestone	

References

- Chen, X.; Shu, L.; Santosh, M. Late Paleozoic post-collisional magmatism in the Eastern Tianshan Belt, Northwest China: New insights from geochemistry, geochronology and petrology of bimodal volcanic rocks. *Lithos* **2011**, *127*, 581–598. [[CrossRef](#)]
- Jahn, B.; Wu, F.; Chen, B. Massive granitoid generation in Central Asia: Nd isotope evidence and implication for continental growth in the Phanerozoic. *Episodes* **2000**, *23*, 82–92. [[CrossRef](#)]
- Long, X.; Yuan, C.; Sun, M.; Xiao, W.; Wang, Y.; Cai, K.; Jiang, Y. Geochemistry and Nd isotopic composition of the Early Paleozoic flysch sequence in the Chinese Altai, Central Asia: Evidence for a northward-derived mafic source and insight into Nd model ages in accretionary orogen. *Gondwana Res.* **2012**, *22*, 554–566. [[CrossRef](#)]
- Memtimin, M.; Pe-Piper, G.; Piper, D.J.W.; Guo, Z.; Zhang, Y. Carboniferous arc-related volcanism in SW Bogda Mountain, Northwest China, and its implications for regional tectonics. *Lithos* **2020**, *360–361*, 105413. [[CrossRef](#)]
- Sengör, A.M.C.; Natal'in, B.A.; Burtman, V.S. Evolution of the Altaid Tectonic Collage and Paleozoic Crustal growth in Eurasia. *Nature* **1993**, *364*, 299–307. [[CrossRef](#)]
- Shu, L.; Wang, B.; Zhu, W.; Guo, Z.; Charvet, J.; Zhang, Y. Timing of initiation of extension in the Tianshan, based on structural, geochemical and geochronological analyses of bimodal volcanism and olistostrome in the Bogda Shan (NW China). *Int. J. Earth Sci.* **2011**, *100*, 1647–1663. [[CrossRef](#)]
- Simonov, V.; Mikolaichuk, A.; Safonova, I.; Kotlyarov, A.; Kovyazin, S. Late Paleozoic-Cenozoic intra-plate continental basaltic magmatism of the Tianshan-Junggar region in the SW Central Asian Orogenic Belt. *Gondwana Res.* **2015**, *27*, 1646–1666. [[CrossRef](#)]
- Wali, G.; Wang, B.; Cluzel, D.; Zhong, L. Carboniferous—Early Permian magmatic evolution of the Bogda range (Xinjiang, NW China): Implications for the late paleozoic accretionary tectonics of the SW central Asian orogenic belt. *J. Asian Earth Sci.* **2018**, *153*, 238–251. [[CrossRef](#)]
- Wang, Q.; Zhao, G.; Han, Y.; Yao, J. Detrital zircon constraints on late Paleozoic tectonism of the Bogda region (NW China) in the southern Central Asian Orogenic Belt. *Geosci. Front.* **2020**, *11*, 1533–1548. [[CrossRef](#)]
- Windley, B.F.; Alexeiev, D.; Xiao, W.J.; Kroner, A.; Badarch, G. Tectonic models for accretion of the Central Asian Orogenic Belt. *J. Geol. Soc.* **2007**, *164*, 31–47. [[CrossRef](#)]
- Xia, L.-Q.; Xia, Z.-C.; Xu, X.-Y.; Li, X.-M.; Ma, Z.-P. Relative contributions of crust and mantle to the generation of the Tianshan Carboniferous rift-related basic lavas, northwestern China. *J. Asian Earth Sci.* **2008**, *31*, 357–378. [[CrossRef](#)]
- Xia, L.; Li, X. Revisiting the tectonic setting of the Carboniferous volcanic rocks in the Chinese Tianshan and its neighboring areas. *Gondwana Res.* **2020**, *84*, 1–19. [[CrossRef](#)]
- Xiao, W.; Han, C.; Yuan, C.; Sun, M.; Lin, S.; Chen, H.; Li, Z.; Li, J.; Sun, S. Middle Cambrian to Permian subduction-related accretionary orogenesis of northern Xinjiang, NW China: Implications for the tectonic evolution of central Asia. *J. Asian Earth Sci.* **2008**, *32*, 102–117. [[CrossRef](#)]
- Xie, W.; Luo, Z.Y.; Xu, Y.G.; Chen, Y.B.; Hong, L.B.; Ma, L.; Ma, Q. Petrogenesis and geochemistry of the late Carboniferous rear-arc (or back-arc) pillow basaltic lava in the Bogda Mountains, Chinese North Tianshan. *Lithos* **2016**, *244*, 30–42. [[CrossRef](#)]
- Xie, W.; Xu, Y.G.; Luo, Z.Y.; Chen, Y.B.; Liu, H.Q.; Hong, L.B.; Ma, L. Petrogenesis and geodynamic implications of the late Carboniferous felsic volcanics in the Bogda belt, Chinese Northern Tianshan. *Gondwana Res.* **2016**, *39*, 165–179. [[CrossRef](#)]
- Zhang, X.; Zhao, G.; Eizenhöfer, P.R.; Sun, M.; Han, Y.; Hou, W.; Liu, D.; Wang, B.; Liu, Q.; Xu, B. Latest Carboniferous closure of the Junggar Ocean constrained by geochemical and zircon U–Pb–Hf isotopic data of granitic gneisses from the Central Tianshan block, NW China. *Lithos* **2015**, *238*, 26–36. [[CrossRef](#)]
- Carroll, A.R.; Liang, Y.; Graham, S.A.; Xiao, X.; Hendrix, M.S.; Chu, J.; McKnight, C.L. Junggar basin, northwest China: Trapped Late Paleozoic Ocean. *Tectonophysics* **1990**, *181*, 1–14. [[CrossRef](#)]
- Carroll, A.R.; Graham, S.A.; Hendrix, M.S.; Ying, D.; Zhou, D. Late Paleozoic tectonic amalgamation of northwestern China Sedimentary record of the northern Tarim, northwestern Turpan, and southern Junggar Basins. *GSA Bull.* **1995**, *107*, 571–594. [[CrossRef](#)]

19. Gao, Y.; Huang, H.; Tao, H.; Carroll, A.R.; Qin, J.; Chen, J.; Yuan, X.; Wang, C. Paleoenvironmental setting, mechanism and consequence of massive organic carbon burial in the Permian Junggar Basin, NW China. *J. Asian Earth Sci.* **2020**, *194*, 104222. [[CrossRef](#)]
20. Liu, D.; Zhang, C.; Yao, E.; Song, Y.; Jiang, Z.; Luo, Q. What generated the Late Permian to Triassic unconformities in the southern Junggar Basin and western Turpan Basin; tectonic uplift, or increasing aridity? *Palaeogeogr. Palaeoclimatol. Palaeoecol.* **2017**, *468*, 1–17. [[CrossRef](#)]
21. Wartes, M.A.; Carroll, A.R.; Greene, T.J.; Cheng, K.; Ting, H. Permian Lacustrine Deposits of Northwest China. In *Lake Basins through Space and Time: AAPG, Studies in Geology*; Gierlowski-Kordesch, E., Kelts, K., Eds.; AAPG, 2000; Volume 46, pp. 123–132. Available online: <http://www.geology.wisc.edu/~jcarroll/publications/pdf/Wartes%20et%20al.,%202000.pdf> (accessed on 15 August 2021).
22. Wartes, M.A.; Carroll, A.R.; Greene, T.J. Permian sedimentary record of the Turpan-Hami basin and adjacent regions, northwest China: Constraints on post-amalgamation tectonic evolution. *GSA Bull.* **2002**, *114*, 131–152. [[CrossRef](#)]
23. Carroll, A.R.; Brassell, S.C.; Graham, S.A. Upper Permian lacustrine oil shales, Southern Junggar Basin, Northwest China. *AAPG Bull.* **1992**, *76*, 1874–1902.
24. Carroll, A.R. Upper Permian lacustrine organic facies evolution, Southern Junggar Basin, NW China. *Org. Chem.* **1998**, *28*, 649–667. [[CrossRef](#)]
25. Huang, H.P. The Nature and Origin of Petroleum in the Chaiwopu Sub-Basin (Junggar Basin), NW China. *J. Pet. Geol.* **2000**, *23*, 193–220. [[CrossRef](#)]
26. Fang, Y.; Wu, C.; Wang, Y.; Hou, K.; Guo, Z. Topographic evolution of the Tianshan Mountains and their relation to the Junggar and Turpan Basins, Central Asia, from the Permian to the Neogene. *Gondwana Res.* **2019**, *75*, 47–67. [[CrossRef](#)]
27. Li, Y.; Yue, W.; Yu, X.; Huang, X.; Yao, Z.; Song, J.; Shan, X.; Yu, X.; Yang, S. Tectonic Evolution of the West Bogeda: Evidences from Zircon U-Pb Geochronology and Geochemistry Proxies, NW China. *Minerals* **2020**, *10*, 341. [[CrossRef](#)]
28. Obrist-Farner, J.; Yang, W. Provenance and depositional conditions of fluvial conglomerates and sandstones and their controlling processes in a rift setting, mid-Permian lower and upper Quanzijie low order cycles, Bogda Mountains, NW China. *J. Asian Earth Sci.* **2017**, *138*, 317–340. [[CrossRef](#)]
29. Shi, Y.; Ji, H.; Yu, J.; Xiang, P.; Yang, Z.; Liu, D. Provenance and sedimentary evolution from the Middle Permian to Early Triassic around the Bogda Mountain, NW China: A tectonic inversion responding to the consolidation of Pangea. *Mar. Pet. Geol.* **2020**, *114*, 104169. [[CrossRef](#)]
30. Tang, W.; Zhang, Z.; Li, J.; Li, K.; Chen, Y.; Guo, Z. Late Paleozoic to Jurassic tectonic evolution of the Bogda area (northwest China): Evidence from detrital zircon U-Pb geochronology. *Tectonophysics* **2014**, *626*, 144–156. [[CrossRef](#)]
31. Thomas, S.G.; Tabor, N.J.; Yang, W.; Myers, T.S.; Yang, Y.; Wang, D. Palaeosol stratigraphy across the Permian–Triassic boundary, Bogda Mountains, NW China: Implications for palaeoenvironmental transition through earth’s largest mass extinction. *Palaeogeogr. Palaeoclimatol. Palaeoecol.* **2011**, *308*, 41–64. [[CrossRef](#)]
32. Wang, J.; Cao, Y.-C.; Wang, X.-T.; Liu, K.-Y.; Wang, Z.-K.; Xu, Q.-S. Sedimentological constraints on the initial uplift of the West Bogda Mountains in Mid-Permian. *Sci. Rep.* **2018**, *8*, 1453. [[CrossRef](#)]
33. Wang, J.; Wu, C.; Li, Z.; Zhu, W.; Zhou, T.; Wu, J.; Wang, J. The tectonic evolution of the Bogda region from Late Carboniferous to Triassic time: Evidence from detrital zircon U-Pb geochronology and sandstone petrography. *Geol. Mag.* **2018**, *155*, 1063–1088. [[CrossRef](#)]
34. Wang, J.; Wu, C.; Zhou, T.; Zhu, W.; Zhou, Y.; Jiang, X.; Yang, D. Source-to-sink analysis of a transtensional rift basin from syn-rift to uplift stages. *J. Sediment. Res.* **2019**, *89*, 335–352. [[CrossRef](#)]
35. Yang, W.; Feng, Q.; Liu, Y.; Tabor, N.; Miggins, D.; Crowley, J.L.; Lin, J.; Thomas, S. Depositional environments and cyclo- and chronostratigraphy of uppermost Carboniferous–Lower Triassic fluvial–lacustrine deposits, southern Bogda Mountains, NW China—A terrestrial paleoclimatic record of mid-latitude NE Pangea. *Glob. Planet. Chang.* **2010**, *73*, 15–113. [[CrossRef](#)]
36. Zhao, R.; Zhang, J.; Zhou, C.; Zhang, Z.; Chen, S.; Stockli, D.F.; Olariu, C.; Steel, R.; Wang, H. Tectonic evolution of Tianshan-Bogda-Kelameili mountains, clastic wedge basin infill and chronostratigraphic divisions in the source-to-sink systems of Permian–Jurassic, southern Junggar Basin. *Mar. Pet. Geol.* **2020**, *114*, 104200. [[CrossRef](#)]
37. Bhatia, M.R. Rare earth element geochemistry of Australian Paleozoic graywackes and mudrocks: Provenance and tectonic control. *Sediment. Geol.* **1985**, *45*, 97–113. [[CrossRef](#)]
38. Bhatia, M.R.; Crook, K.A.W. Trace element characteristics of graywackes and tectonic setting discrimination of sedimentary basins. *Contrib. Mineral. Petrol.* **1986**, *92*, 181–193. [[CrossRef](#)]
39. Cox, R.; Lowe, D.R.; Cullers, R.L. The influence of sediment recycling and basement composition on evolution of mudrock chemistry in the southwestern United States. *Geochim. Cosmochim. Acta* **1995**, *59*, 2919–2940. [[CrossRef](#)]
40. Dickinson, W.R. Interpreting provenance relations from detrital modes of Sandstones. In *Provenance of Arenites*; Zuma, G.G., Ed.; Reidel: Dordrecht, The Netherlands, 1985; pp. 333–361.
41. Fedo, C.M.; Nesbitt, H.W.; Young, G.M. Unravelling the effects of potassium metasomatism in sedimentary rocks and paleosols, with implications for paleo-weathering conditions and provenance. *Geology* **1995**, *23*, 921–924. [[CrossRef](#)]
42. Floyd, P.A.; Winchester, J.A.; Park, R.G. Geochemistry and tectonic setting of Lewisian clastic metasediments from the early Proterozoic Lock Marie Group of Gairloch, Scotland. *Precambrian Res.* **1989**, *45*, 203–214. [[CrossRef](#)]

43. Herron, M.M. Geochemical classification of terrigenous sands and shales from core or log data. *J. Sediment. Petrol.* **1988**, *58*, 820–829. [[CrossRef](#)]
44. Le Bas, M.J.; Le Maitre, R.W.; Streckeisen, A.; Zanettin, B. A chemical classification of volcanic rocks based on the total alkali-silica diagram. *J. Petrol.* **1986**, *27*, 745–750. [[CrossRef](#)]
45. McLennan, S.M.; McLennan, S.M.; Hemming, S.; McDaniel, D.K.; Hanson, G.N. Geochemical approaches to sedimentation, provenance and tectonics. In *Processes Controlling the Composition of Clastic Sediments*; Johansson, M.J., Basu, A., Eds.; Geological Society America: Boulder, CO, USA, 1993; Volume 284, pp. 21–40. [[CrossRef](#)]
46. Nesbitt, H.W.; Young, G.M. Early Proterozoic climates and plate motions inferred from major element chemistry of lutites. *Nature* **1982**, *299*, 715–717. [[CrossRef](#)]
47. Pearce, J.A. Trace element characteristics of lavas from destructive plate boundaries. In *Andesites*; Thorps, R.S., Ed.; John Wiley and Sons: New York, NY, USA, 1982; pp. 525–548.
48. Roser, B.P.; Korsch, R.J. Determination of tectonic setting of sandstone–mudstone suites using SiO₂ content and K₂O/Na₂O ratio. *J. Geol.* **1986**, *94*, 635–650. [[CrossRef](#)]
49. Roser, B.P.; Cooper, R.A.; Nathan, S.; Tulloch, A.J. Reconnaissance sandstone geochemistry, provenance, and tectonic setting of the lower Paleozoic terranes of the West Coast and Nelson, New Zealand. *N. Z. J. Geol. Geophys.* **1996**, *39*, 1–16. [[CrossRef](#)]
50. Roser, B.P.; Korsch, R.J. Provenance signatures of sandstone–mudstone suites determined using discrimination function analysis of major-element data. *Chem. Geol.* **1988**, *67*, 119–139. [[CrossRef](#)]
51. Suttner, L.J.; Dutta, P.K. Alluvial sandstone composition and paleoclimate, framework mineralogy. *J. Sediment. Petrol.* **1986**, *56*, 329–345. [[CrossRef](#)]
52. Taylor, S.R.; McLennan, S.M. *The Continental Crust: Its Composition and Evolution*; Blackwell Scientific Publications: Oxford, UK, 1985; p. 312.
53. Verma, S.P.; Armstrong-Altrin, J.S. New multi-dimensional diagrams for tectonic discrimination of siliciclastic sediments and their application to Precambrian basins. *Chem. Geol.* **2013**, *355*, 117–133. [[CrossRef](#)]
54. Dobretsov, N.L.; Berzin, N.A.; Buslov, M.M. Opening and tectonic evolution of the Paleo-Asian Ocean. *Int. Geol. Rev.* **1995**, *37*, 335–360. [[CrossRef](#)]
55. Safonova, I.; Kotlyarov, A.; Krivonogov, S.; Xiao, W. Intra-oceanic arcs of the Paleo-Asian ocean. *Gondwana Res.* **2017**, *50*, 167–194. [[CrossRef](#)]
56. Wan, B.; Li, S.; Xiao, W.; Windley, B.F. Where and when did the Paleo-Asian ocean form? *Precambrian Res.* **2018**, *317*, 241–252. [[CrossRef](#)]
57. Haq, B.U.; Schutter, S.R. A Chronology of Paleozoic Sea-Level Changes. *Science* **2008**, *322*, 64–68. [[CrossRef](#)]
58. BGMRXUAR (Bureau of Geology and Mineral Resources of Xinjiang Uygur Autonomous Region). *Regional Geology of Xinjiang Uygur Autonomous Region*; Geological Publishing House: Beijing, China, 1993; p. 841. (in Chinese with English summary)
59. Xue, D.; Wang, H.; Liu, Y.; Xie, L.; Shen, P. An Improved Procedure for the Determination of Ferrous Iron Mass Fraction in Silicate Rocks Using a Schlenk Line-Based Digestion Apparatus to Exclude Oxygen. *Geostand. Geoanalytical Res.* **2017**, *41*, 411–425. [[CrossRef](#)]
60. Bouma, A.H. *Sedimentology of Some Flysch Deposits: A Graphic Approach to Facies Interpretation*; Elsevier Publishing Company: Amsterdam, The Netherlands; New York, NY, USA, 1962; p. 168.
61. Babechuk, M.G.; Widdowson, M.; Kamber, B.S. Quantifying chemical weathering intensity and trace element release from two contrasting basalt profiles, Deccan Traps, India. *Chem. Geol.* **2014**, *363*, 56–75. [[CrossRef](#)]
62. Lee, E.Y.; Tejada, M.L.G.; Song, I.; Chun, S.S.; Gier, S.; Riquier, L.; White, L.T.; Schnetger, B.; Brumsack, H.-J.; Jones, M.M.; et al. Petrophysical Property Modifications by Alteration in a Volcanic Sequence at IODP Site U1513, Naturaliste Plateau. *J. Geophys. Res. Solid Earth* **2021**, *126*, e2020JB021061. [[CrossRef](#)]
63. Morgan, J.; Moore, K.; Moore, G.F.; Clague, D.A. Slope failure and volcanic spreading along the submarine south flank of Kilauea volcano, Hawaii. *J. Geophys. Res. Solid Earth* **2003**, *108*, 2415. [[CrossRef](#)]
64. Muravchik, M.; Bilmes, A.; D’Elia, L.; Franzese, J.R. Alluvial fan deposition along a rift depocentre border from the Neuquén Basin, Argentina. *Sediment. Geol.* **2014**, *301*, 70–89. [[CrossRef](#)]
65. Gawthorpe, R.L.; Leeder, M.R. Tectono-sedimentary evolution of active extensional basins. *Basin Res.* **2000**, *12*, 195–218. [[CrossRef](#)]
66. Alexander, J.; Leeder, M.R. Geomorphology and surface tilting in an active extensional basin, SW Montana, USA. *J. Geol. Soc.* **1990**, *147*, 461–467. [[CrossRef](#)]
67. Kim, Y.; Huh, M.; Lee, E.Y. Numerical Modelling to Evaluate Sedimentation effects on Heat Flow and Subsidence during Continental Rifting. *Geosciences* **2020**, *10*, 451. [[CrossRef](#)]
68. Zou, C.; Wang, L.; Li, Y.; Tao, S.; Hou, L. Deep-lacustrine transformation of sandy debrites into turbidites, Upper Triassic, Central China. *Sediment. Geol.* **2012**, *265–266*, 143–155. [[CrossRef](#)]
69. Knierzinger, W.; Wagreich, M.; Palzer-Khomenko, M.; Gier, S.; Meszar, M.; Lee, E.Y.; Koukal, V.; Strauss, P. Provenance and palaeogeographic evolution of Lower Miocene sediments in the eastern North Alpine Foreland Basin. *Swiss J. Geosci.* **2019**, *112*, 269–286. [[CrossRef](#)]